

EFFECTS OF
FILM AND CONVECTION
COOLING ARRANGEMENTS
ON
NGV CAPACITY AND LOSS

A THESIS SUBMITTED FOR THE DEGREE OF
MASTER OF SCIENCE BY RESEARCH
SEPTEMBER 2016



BY
T. M. F. GAMMAGE, ST JOHN'S COLLEGE

Effects of Film and Convection Cooling Arrangements on NGV Capacity and Loss

Thomas M. F. Gammage

September 2016

I wish to give great thanks to everyone at Osney who helped and advised me during my time there, and to my correspondents at Rolls-Royce who made our research possible.

My family and friends outside the lab deserve no less thanks for their support - especially Chris Parton.

Abstract

This thesis describes a series of CFD investigations into how the capacity and loss of high-pressure nozzle guide vanes are affected by various factors. Simulations were designed to answer questions about the effects of design and manufacturing variables, but also to answer questions about which CFD techniques are most effective in predicting the physical effects that underpin NGV performance.

CFD predictions were made about the effects of varying the geometry of NGV cooling arrangements. These variations included the position of a single suction-side cooling hole and the shape of the trailing-edge slot of the NGV. The effects of varying trailing-edge slot blowing rate were also investigated.

A comparison was made between the predictions of the single-cooling-hole positioning study in 2D and quasi-3D CFD. This was used to draw conclusions about the importance of mixing in film cooling aerodynamics, and to comment on the relative effectiveness of the 2 CFD approaches. A comparison was also made between the relative effectiveness of steady and unsteady CFD in making capacity predictions as part of the variable suction-side cutbacks study.

The effects of manufacturing variations on the capacity of NGVs were considered using geometric scans of parts provided by Rolls-Royce. By running 2D CFD, conclusions were also drawn about which of these effects are best predicted by 2D CFD and which by 3D CFD.

Contents

1	Introduction - Background of Capacity	15
2	Literature Review	17
2.1	Capacity Prediction and Measurement	17
2.2	Cooling, Capacity and Loss	17
3	Capacity CFD Predictions	21
3.1	Single Film Cooling Row Positioning - 2D Study	21
3.1.1	Geometry	21
3.1.2	Boundary Conditions	23
3.1.3	Mesh	23
3.1.4	Simulation	25
3.1.5	Results	25
3.1.6	Comparison of Spalart-Allmaras and SST $k-\omega$ Turbulence Models	29
3.2	Single Film Cooling Row Positioning - Quasi-3D Study	30
3.2.1	Geometry	30
3.2.2	Boundary Conditions	30
3.2.3	Mesh	31
3.2.4	Simulation	32
3.2.5	Results	32
3.3	2D Capacity of Trent 900 Smooth NGVs	35
3.3.1	Geometry	35
3.3.2	Boundary Conditions	36
3.3.3	Mesh	36
3.3.4	Simulation	37
3.3.5	Results	38
3.4	Effects of Trailing Edge Design on Capacity	41
3.4.1	Pressure-Side Cutback Geometry	42

3.4.2	Suction-Side Cutback Geometry	43
3.4.3	Boundary Conditions and Steady-State Simulation	45
3.4.4	Pressure-Side Cutback Mesh	45
3.4.5	Suction-Side Cutback Mesh	47
3.4.6	Unsteady Simulation and Mesh Modification	47
3.4.7	Blowing Rate Variation	48
3.4.8	Results	48
3.5	Conclusions	57

List of Figures

2.1	Separated contributions to loss, Raffel and Kost	20
3.1	Process for preparing 2D NGV profile	22
3.2	23
3.3	24
3.4	Total capacity percentage delta as a function of single cooling hole position	26
3.5	27
3.6	28
3.7	Details of mesh for single-cooling-hole quasi-3D study	31
3.8	Detail of cooling hole mesh for quasi-3D study	32
3.9	Development of entropy downstream of a single suction-side cooling hole, 2D and quasi-3D	33
3.10	NGV surface contours of specific entropy, quasi-3D	33
3.11	34
3.12	Mesh for Trent 900 smooth-vane capacity study	37
3.13	38
3.14	39
3.15	Mach 1 contours for 6 scanned Trent 900 NGVs	40
3.16	Design of Trent 900 centred-ejection geometry	42
3.17	Trailing-edge cut-back scheme, r_{cp} values given	43
3.18	Changes to Rolls-Royce trailing-edge geometry for this study	44
3.19	Cutback scheme for suction-side study	45
3.20	NGV mesh for centred-ejection study	46
3.21	Trailing-edge meshes for centred-ejection study, r_{cp} values given	46
3.22	NGV mesh for suction-side cutback study	47
3.23	49
3.24	Energy loss as a function of suction-side cutback r_{cs}	50
3.25	Contours of Mach number for $r_{cp} = 0, 1, 2, 3$ and $PR = 1.79, 3.33$	51
3.26	Contours of Mach number for $r_{cs} = 0, 2, 4, 6, 8, 10$ and $PR = 1.79$	52
3.27	53

3.28	54
3.29	55
3.30	Filtered history of integrated static pressure on the vane surface in unsteady simulation	56
3.31	57

List of Tables

3.1	Simulation Parameters	25
3.2	Trent 900 scanned vanes	36
3.3	Simulation Parameters	38

Nomenclature

Romans

M	Mach number
\dot{m}	Mass flow rate
A	Throat area
p_0	Total pressure
T_0	Total temperature
R	Gas constant, $0.287 \text{ kJkg}^{-1}\text{K}^{-1}$
p	Static pressure
h	Enthalpy
h_0	Stagnation enthalpy
W	Area-averaged flow velocity
C_p	Pressure coefficient
r_c	Cutback ratio

Greeks

γ	Ratio of specific heats, 1.4
Γ	NGV flow capacity
Δ	Change in quantity
ζ	Energy loss coefficient (Raffel and Kost)
ρ	Gas density

Acronyms and Abbreviations

NGV	Nozzle guide vane
1D	One-dimensional
PR	NGV pressure ratio
3D	Three-dimensional
2D	Two-dimensional
CFD	Computational fluid dynamics
TE	Trailing edge
KE	Kinetic energy
XWB	Extra wide body
84K	84,000 lbs thrust
FMG	Full multi-grid
SST	Shear stress transport
HP	High-pressure
RANS	Reynolds-averaged Navier-Stokes
URANS	Unsteady Reynolds-averaged Navier-Stokes

Subscripts

1	Inlet
2	Outlet
<i>is</i>	Isentropic
<i>tota</i>	Normalised against NGV inlet conditions
<i>totb</i>	Normalised against NGV inlet and coolant inlet conditions
<i>p</i>	Pressure-side
<i>s</i>	Suction-side

Chapter 1

Introduction - Background of Capacity

Coolant airflow is essential to modern gas turbines. Engines could not run at such high temperatures and efficiencies without it, but its presence adversely affects efficiency by compromising the aerodynamics of the cooled blades and vanes. Different cooling arrangements for high-pressure nozzle guide vanes (NGVs) can result in different effects on the flow capacity and losses. Incomplete understanding of these effects results in significant penalties on overall engine efficiency.

Incorrect prediction of the mass flow rate through the annulus of NGVs results in mismatching of downstream turbine stages. This error is compounded with each subsequent stage. The consequence is a significant discrepancy between engine design efficiency and real efficiency. It is therefore important to predict NGV mass flow rate as accurately as possible.

1D isentropic mass flow rate through a nozzle can be given by

$$M < 1 \quad \dot{m} = A \frac{p_{01}}{\sqrt{T_{01}}} \sqrt{\frac{\gamma}{R}} M \left(1 + \frac{\gamma-1}{2} M^2 \right)^{-\frac{\gamma+1}{2(\gamma-1)}} \quad (1.1)$$

$$M \geq 1 \quad \dot{m} = A \frac{p_{01}}{\sqrt{T_{01}}} \sqrt{\frac{\gamma}{R}} \left(1 + \frac{\gamma-1}{2} \right)^{-\frac{\gamma+1}{2(\gamma-1)}} \quad (1.2)$$

where M is throat Mach number, \dot{m} is mass flow rate, A is throat geometric area, and T_{01} and p_{01} are inlet total temperate and total pressure respectively.

It is convenient to normalise NGV mass flow rate against inlet total pressure and total temperature. With no cooling, capacity is thus defined as

$$\Gamma = \dot{m} \frac{\sqrt{T_{01}}}{p_{01}} \quad (1.3)$$

NGV mass flow rate can then be expressed independently of upstream total temperature and pressure, using capacity as

$$M < 1 \quad \Gamma = A \left(\frac{p_2}{p_{01}} \right)^{\frac{\gamma+1}{2\gamma}} \sqrt{\frac{\gamma}{R}} \sqrt{\left[\left(\frac{p_2}{p_{01}} \right)^{\frac{1-\gamma}{\gamma}} - 1 \right] \frac{2}{\gamma-1}} \quad (1.4)$$

$$M = 1 \quad \Gamma = A \sqrt{\frac{\gamma}{R}} \left[1 + \left(\frac{\gamma-1}{2} \right) \right]^{-\frac{(\gamma-1)}{2(\gamma-1)}} \quad (1.5)$$

where p_2 is outlet static pressure. Capacity thus becomes a function of pressure ratio

$$PR = \frac{p_{01}}{p_2} \quad (1.6)$$

This definition of pressure ratio is used for the boundary conditions of all CFD analyses in this thesis.

Measurements of the capacity of NGVs have been performed by Rolls-Royce using their own continuous-running facility. More recently, measurements have been performed in the Oxford Capacity Facility [1][2]. This is a blowdown-type setup that performs transient tests of a complete annulus of NGVs with cooling flow. It offers an order-of-magnitude cost saving compared to the continuous approach previously used at Rolls-Royce.

Chapter 2

A Review - NGV Capacity and Loss

2.1 Capacity Prediction and Measurement

Afanasiev et al [3][4] evaluated the discrepancies between 1D and 3D predictions of the capacities of NGVs. They concluded that these discrepancies are significant enough that full analysis of the performance of a turbine stage should be done in 3D. This work is relevant to the present study because the present study involves coolant/mainstream interactions that are either 2D or 3D in nature, for which 1D analysis would result in inaccurate predictions.

Fielding [5] performed a mathematical analysis of how irreversibility leads to maximum mass flow occurring at a Mach number slightly below unity. The work developed a method of applying boundary layer theory to 1D capacity predictions. The method resulted in 1D estimates of blade row capacity which are in good agreement with experimental results. The work will inform future analytical capacity predictions resulting from the present study.

2.2 Effects of Film and Convection Cooling on NGV Capacity and Loss

Walters and Leylek [6] studied the effects of film cooling on profile loss (as opposed to end-wall loss). Their aim was to discern effectively the ability of CFD methods to predict loss, by comparing their predictions with an experimental test case. They found that the use of an appropriate turbulence model was crucial to avoid significant errors, and recommended either the Reynolds stress model or the realisable k- ϵ model. At low coolant injection rates mixing loss was dominant. At

higher rates they suggested that injection initiated boundary layer transition and changes in loss in the boundary layer may become significant. They also found that coolant/mainstream density ratio had a negligible effect on loss. The experiments and computations were matched in terms of inlet total temperature, coolant blowing rate, and exit Mach number. This work is of relevance to the 2D film cooling CFD in the present study.

Denton and Xu [7] performed an analytical and numerical study of trailing edge loss. They found that base pressure and trailing edge loss can be predicted without considering viscous effects. This is because viscous effects were found to only modify the solution by changing the pressure distribution on the suction surface downstream of the throat. This work will inform future analytical and numerical capacity predictions resulting from the present study.

Deckers and Denton [8] tested the effects of TE slot ejection using flat or nearly flat plates. They found that coolant total temperature ratio has an insignificant effect on base pressure and loss. Their tests on solid trailing edges demonstrated that the KE loss coefficient increased up to approximately $M = 1$ due to shock and boundary layer losses. For Mach numbers above unity the overall loss was found to decrease drastically. This unusual result was caused primarily by changes in the trailing edge shock system which influenced the strength and position of the shock interaction with the suction surface boundary layer. The tests on TEs with slots demonstrated that the existence of an un-blown slot increased base pressure by 25% and reduced loss by 30%. Relative to this un-blown slotted case, a blown slot increased base pressure by up to a further 42% with loss down a further 44%. Minimum loss and maximum base pressure did not occur at the same coolant ejection rate. Minimum loss was obtained when coolant ejection rate was 1% of the main flow. Loss definition accounted for the coolant potential energy. This work may be compared to the numerical predictions of the effects of TE slot ejection on loss in the present study.

Kost and Holmes [9] used a rectilinear cascade to test two designs of turbine blade designed by Rolls-Royce. One blade had a thin trailing edge with ejection from a row of angled cylindrical holes on the suction side and a row of smaller holes on the pressure side; the other had a thick trailing edge with a central slot. Tests were performed at design exit Mach number of 1.15. It was found that the introduction of a moderate amount of coolant from the row of holes into subsonic local flow caused a decrease in loss. Injection of supersonic coolant into subsonic main flow or injecting coolant into supersonic main flow caused an increase in loss. Comparison of the two blade designs suggested that a blade with a thick trailing edge and coolant ejection into the base region may be similar in performance to a blade with a much thinner trailing edge and film cooling just before the trailing edge, if the blades are compared at higher coolant flow rates. This work may be compared to the numerical predictions of the effects of TE slot ejection

on loss in the present study.

Raffel and Kost [10] experimentally investigated a flat plate with trailing edge slot ejection at different coolant flow rates. Energy loss as defined by Horlock [11] (not accounting for coolant energy) was defined as

$$\xi = 1 - \frac{h_{02} - h_2}{h_{01} - h_{2is}} = 1 - \frac{W_2^2}{W_{2is}^2} = 1 - \frac{1 - (\frac{p_2}{p_{02}})^{\frac{\gamma-1}{\gamma}}}{1 - (\frac{p_2}{p_{01}})^{\frac{\gamma-1}{\gamma}}} \quad (2.1)$$

where h_{02} is outlet stagnation enthalpy, h_2 is outlet enthalpy, h_{01} is inlet stagnation enthalpy, h_{2is} is outlet isentropic enthalpy, W_2 is outlet average flow velocity, W_{2is} is outlet average isentropic flow velocity, p_2 and p_{02} are the outlet flow static and total pressures.

In addition to pressure measurements, particle image velocimetry was used to investigate the instantaneous velocity field. Loss contributions were separated into upstream profile losses and coolant flow mixing losses. This was achieved by dividing the flow into the main flow region, the base regions and the slot exit region. Measurements of pressure were taken upstream of the trailing edge, in the base region, and well downstream of the trailing edge. Separated contributions to loss are shown in Figure 2.1. Measured losses displayed a maximum at a downstream isentropic Mach number of 1. This was strongly related to the behaviour of the base pressure. It was found that losses could be reduced at a certain low mass flow rate of coolant. Losses increased again at higher coolant mass flow rates. It was also concluded that a vortex street exists downstream of the trailing edge, even in the case of supersonic exit Mach numbers. This vortex street can be suppressed by trailing edge coolant ejection at low flow rates.

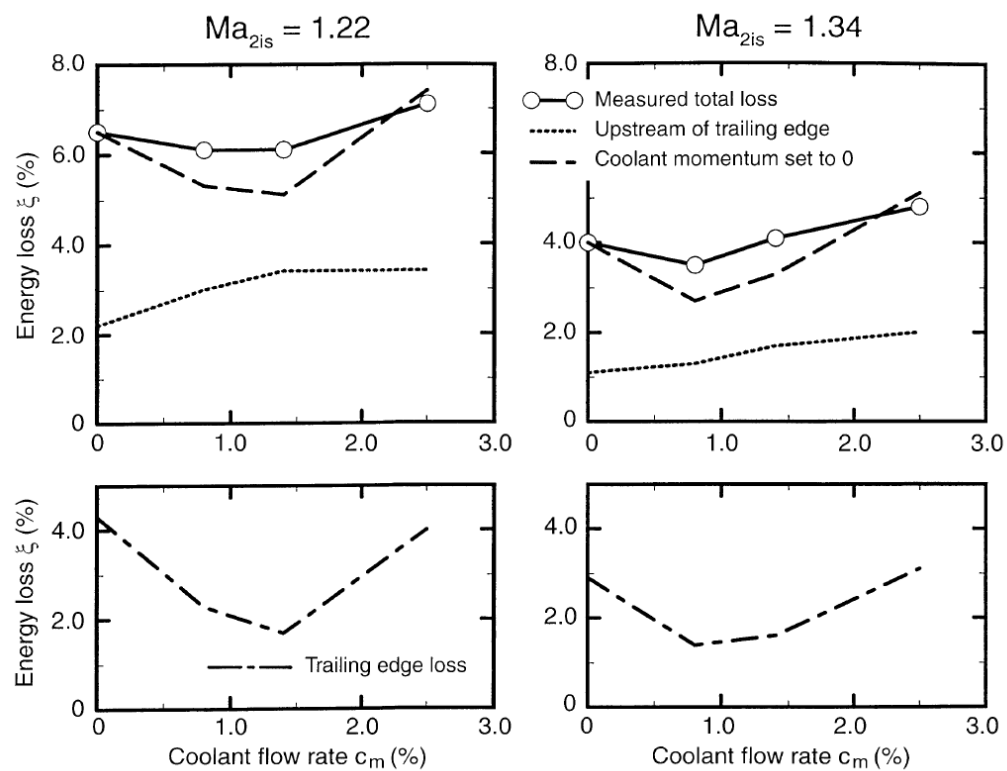


Figure 2.1: Separated contributions to loss, Raffel and Kost

Chapter 3

Capacity CFD Predictions

This chapter presents CFD investigations into how variation of the geometries of film and convection cooling arrangements affects NGV capacity. Location of a suction-side film cooling row is found to have a small but significant effect. Size of a pressure-side trailing edge slot cutback is found to have a linear effect.

A comparison is made between the use of two different turbulence models in 2D CFD. The two are found to give similar capacity predictions but flow-fields that slightly differ near the trailing edge and film cooling hole.

Significant differences between 2D and 3D CFD capacity predictions are discussed. It is found that there are phenomena in 3D which are not captured in 2D. It is also found that there are phenomena in 2D which are difficult to isolate in 3D. It is concluded that 3D investigations are important but capacity characteristics result predominantly from 2D phenomena.

3.1 Single Film Cooling Row Positioning - 2D Study

Rolls-Royce identified a possible requirement for an additional row of film cooling holes to be added to the suction-side of Trent XWB NGVs. A 2D CFD study was performed to predict the effects of single cooling row location on NGV capacity and aerodynamics. Because the study was 2D, the cooling row was modelled as a single straight-sided passage. The study was performed in ANSYS Fluent. Results were analysed in MATLAB.

3.1.1 Geometry

The vane profile used for this study was the Rolls-Royce Trent XWB 84K standard with a rounded trailing edge. The aerodynamic definition of this geometry was

provided by Rolls-Royce as a set of co-ordinates which define 21 streamlines on the vane surface. The 11th streamline was considered to be nearest to mid-span.

MATLAB was used to process the 3D curve of the 11th streamline to produce a 2D section. The 3D co-ordinate system was cylindrical. The origin was the centre of the annulus of NGVs. The 3D curve was projected onto a cylindrical surface whose radius was equal to the NGV annular radius at mid-span. The circumferential and axial co-ordinates were then taken as the x and y co-ordinates of a 2D system. The geometry processing is illustrated in Figure 3.1.

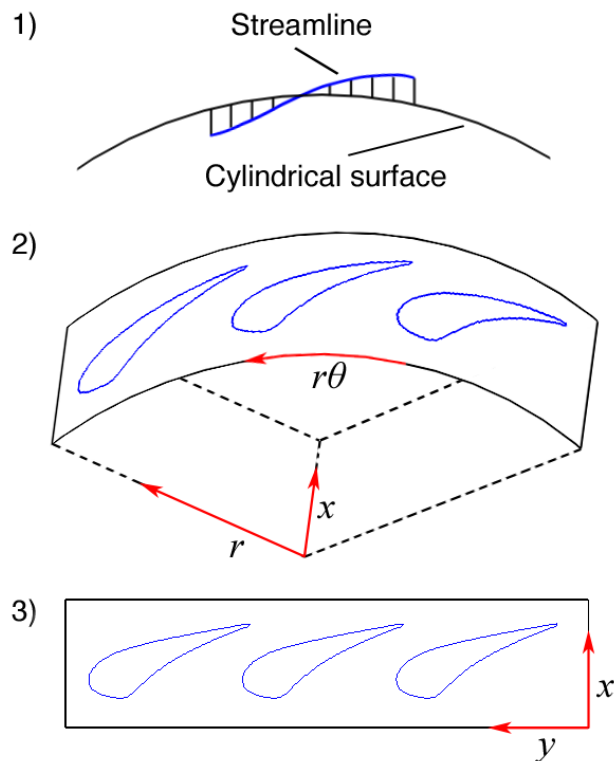


Figure 3.1: Process for preparing 2D NGV profile

The co-ordinates of the NGV unwrapped midsection were connected to form a closed line. This body was placed in a computational domain consisting of a straight inlet section, a curved turning section, and a straight outlet section inclined at the NGV turning angle. The geometry was periodically repeating. The resulting spacing between NGVs was engine-representative. A single cooling hole was modelled as a small straight-sided passage. Because the analysis was 2D, this hole model was equivalent to a section of a slot. Effects due to the circular shape of the real hole were not considered.

3.1.2 Boundary Conditions

The cooling plenum was modelled as a rectangular chamber connected to the cooling hole. The walls of the chamber were set as an inlet. Total pressure was specified at the domain inlet and static pressure was specified at the domain outlet. Both were scalar values with no profiling. Coolant mass flow rate was set to an engine-representative value of 0.3% of mainstream.

The computational domain and boundary conditions are illustrated in Figure 3.2a. The foremost and aftmost cooling hole positions are illustrated in Figure 3.2b, where 0 denotes the furthest upstream and 1 denotes the furthest downstream.

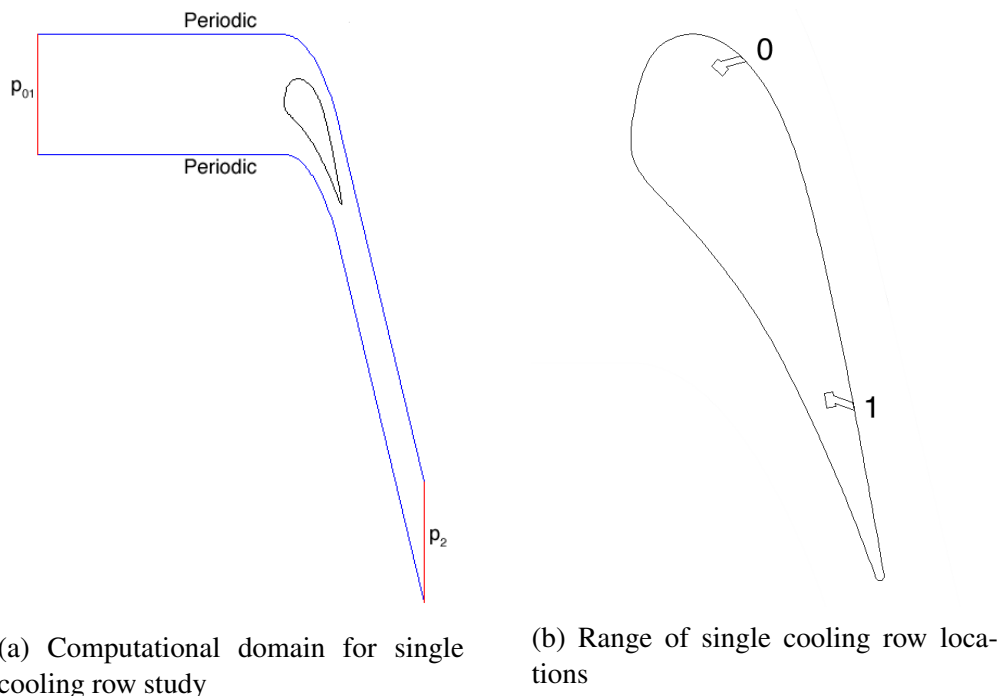


Figure 3.2

3.1.3 Mesh

MATLAB was used to create a closed line whose distance from the vane surface was constant. This distance was equal to the predicted maximum boundary layer thickness plus 15%. The region thus enclosed was set as a structured quadrilateral mesh. Sizing was used to give this mesh a y -plus value of 2.5. This is a typical value when it is desired to resolve the laminar sub-layer [12]. Sizings were used along the vane surface to ensure that the high curvature of the trailing edge ge-

ometry was sufficiently resolved in the mesh. The cooling hole and plenum were each given a rectangular block of structured mesh.

Beyond the structured boundary layer blocks, an unstructured quadrilateral-dominant mesh was used. *Match controls* were used to make the cell spacing along the matching periodic boundaries identical. Cell growth ratio was limited to ensure good resolution downstream of the vane.

The mesh is shown in Figures 3.3a, 3.3b and 3.3c.

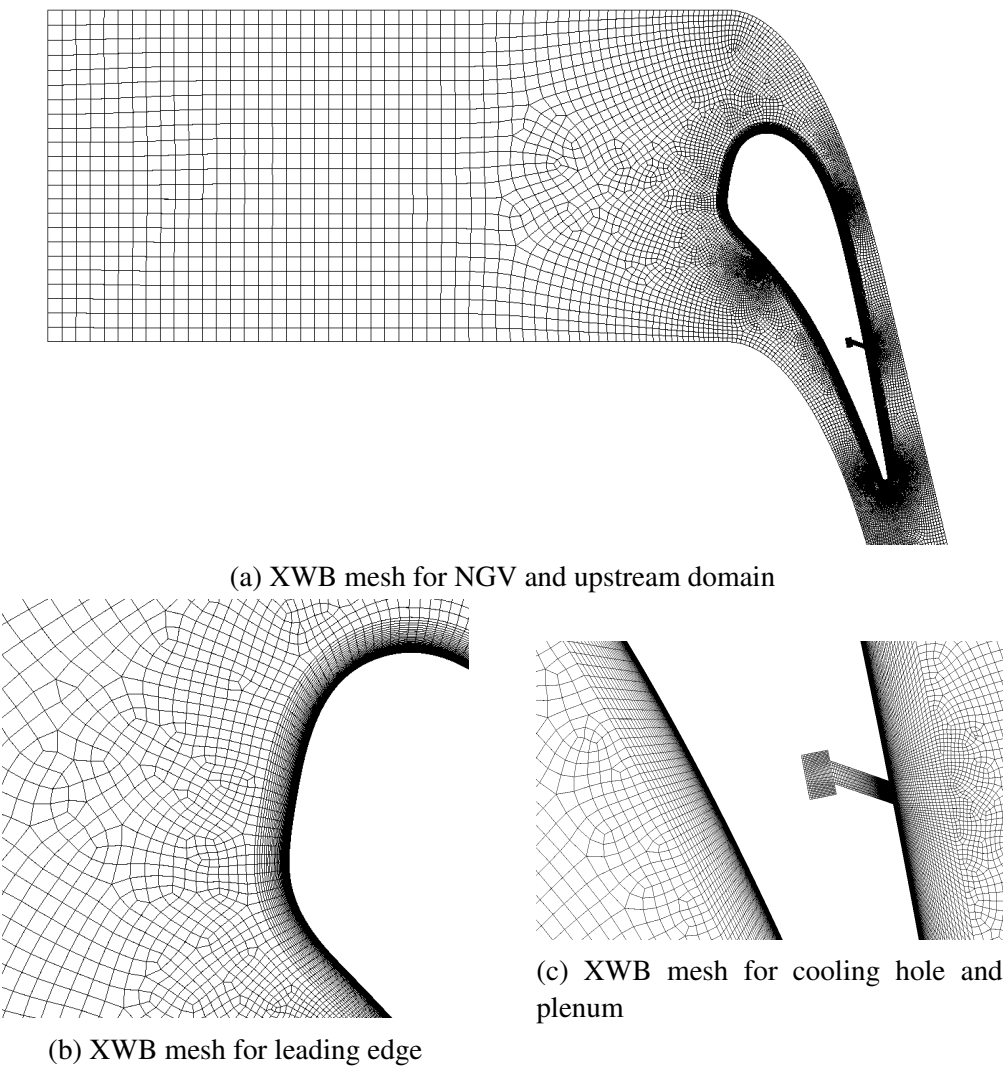


Figure 3.3

3.1.4 Simulation

The FLUENT simulation was controlled using a script written in FLUENT's *Journal* language. The solution was initialised using the FMG method built into the solver. Solutions were then converged at incrementally increasing pressure ratios between 1.01 and the design pressure ratio of 1.65. There were 20 increments and typical overall solution times were approximately 6 hours.

Solutions were computed using both the SST $k-\omega$ [13] and the Spalart-Allmaras [14] turbulence models. This allowed subsequent comparison of the two models.

Simulation parameters are given in Table 3.1.

Table 3.1: Simulation Parameters

Parameter	Value
NGV turning (degrees)	73.969
NGV throat width (m)	1.253×10^{-2}
Design pressure ratio	1.648
Inlet total pressure (Pa)	4.326×10^6
Inlet total temperature (K)	300
Outlet static pressure (Pa)	2.625×10^6
Outlet static temperature (Pa)	300
Coolant/mainstream mass flow ratio	0.003
Solver type	Density-based
Cell count	40,000

3.1.5 Results

Data from FLUENT runs were processed using MATLAB. NGV capacity and vane surface static pressure and surface isentropic Mach number were evaluated for a series of single cooling hole positions. Cooling hole position is referred to in the range 0-1, where 0 is just downstream of the throat and 1 is just upstream of the trailing edge.

When there is coolant flow, capacity may be defined in two ways:

$$\Gamma_{tota} = (\dot{m}_m + \dot{m}_c) \frac{\sqrt{T_{01}}}{p_{01}} \quad (3.1)$$

$$\Gamma_{totb} = \dot{m}_m \frac{\sqrt{T_{0m}}}{p_{0m}} + \dot{m}_c \frac{\sqrt{T_{0c}}}{p_{0c}} \quad (3.2)$$

where subscript m denotes mainstream inlet flow and c denotes coolant inlet flow.

The isentropic Mach number plotted on the vane surface is defined as

$$M_{is} = \sqrt{\frac{2}{\gamma-1} \left[\left(\frac{p_{01}}{p_s} \right)^{\frac{\gamma-1}{\gamma}} - 1 \right]} \quad (3.3)$$

where p_{01} is the inlet total pressure, p_s is the local static pressure, and the ratio of specific heats $\gamma = 1.4$.

Vane surface static pressure coefficient is defined as

$$C_p = \frac{p_s}{p_{01}} \quad (3.4)$$

Effect of Cooling Row Location on Capacity

Total capacity percentage delta is plotted as a function of cooling hole position in Figure 3.4. Results are shown for both the SST k- ω and Spalart-Allmaras turbulence models.

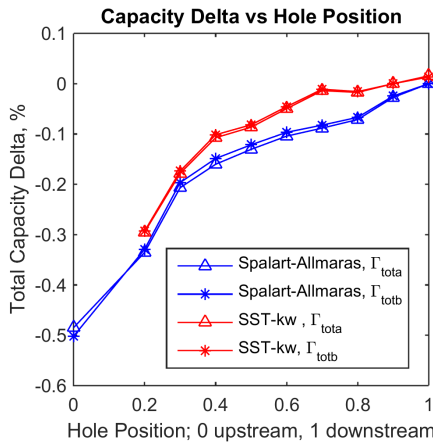


Figure 3.4: Total capacity percentage delta as a function of single cooling hole position

Figure 3.4 shows a characteristic in which capacity increased as the single cooling hole was moved downstream. This was the case for both the SST k- ω and the Spalart-Allmaras turbulence models. The maximum difference between the predictions of the two models was approximately 0.07%. Overall capacity delta between cooling hole position 0 and cooling hole position 1 was approximately 0.5%.

The predicted relationship is most probably dominated by the local mainstream flow speed at the point of coolant injection. Positions further downstream

are injecting into locally slower flow and thus causing less blockage. Comparison of Figures 3.4 and 3.5a shows that this cannot be purely a characteristic of surface isentropic Mach number: this property has its maximum inside the range of cooling row positions. The capacity relationship is likely to be influenced by a combination of surface isentropic Mach number and free-stream Mach number.

Vane Surface Plots

NGV surface isentropic Mach number is plotted as a function of axial position in Figure 3.5a. Figure 3.5a is for the SST $k-\omega$ turbulence model. Surface static pressure coefficient (normalised against inlet total pressure) is plotted as a function of axial position for both turbulence models in Figure 3.5b.

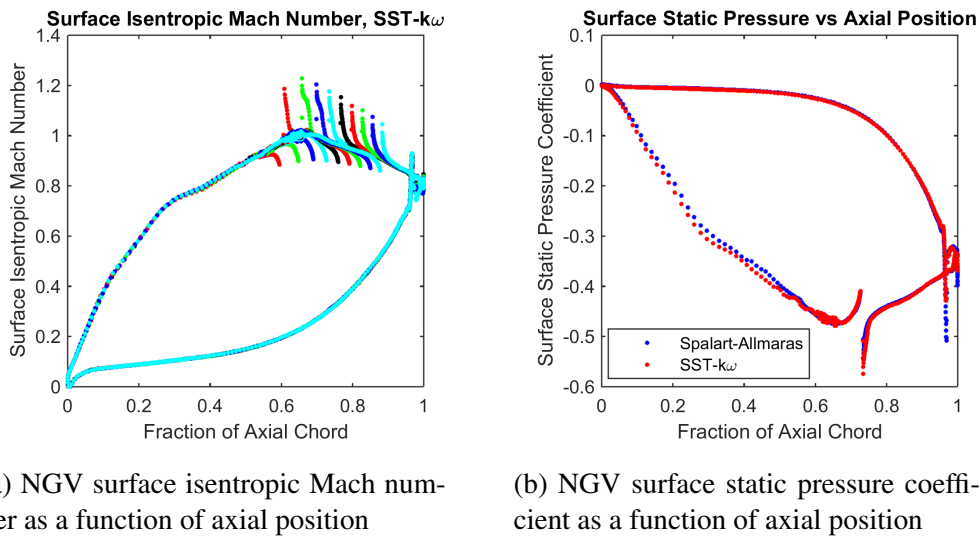


Figure 3.5

Figure 3.5a shows that overall surface isentropic Mach number was unaffected by single cooling hole position. A local sharp rise in surface static pressure was present at the location of the hole. The magnitude of this singularity was largely unaffected by the placement of the hole.

An unusual predicted feature was observed at the pressure-side trailing edge of the NGV in all cases. This local *fast patch* was characterised by a sudden significant decrease in static pressure and corresponding increase in isentropic Mach number at this point on the surface.

Figure 3.5b shows that overall surface static pressure distribution was similar for both turbulence models, particularly on the pressure-side. The most significant difference between the two models was at the *fast patch*. Here the sud-

den decrease in surface static pressure was approximately twice as large with the Spalart-Allmaras turbulence model than with SST $k-\omega$.

CFD Visualisations

Contours of Mach number were computed in FLUENT for the single-cooling-hole solutions. Contours using the SST $k-\omega$ turbulence model are shown in Figure 3.6a. Contours at the vane TE are shown to compare the SST $k-\omega$ and Spalart-Allmaras turbulence models in Figure 3.6b.

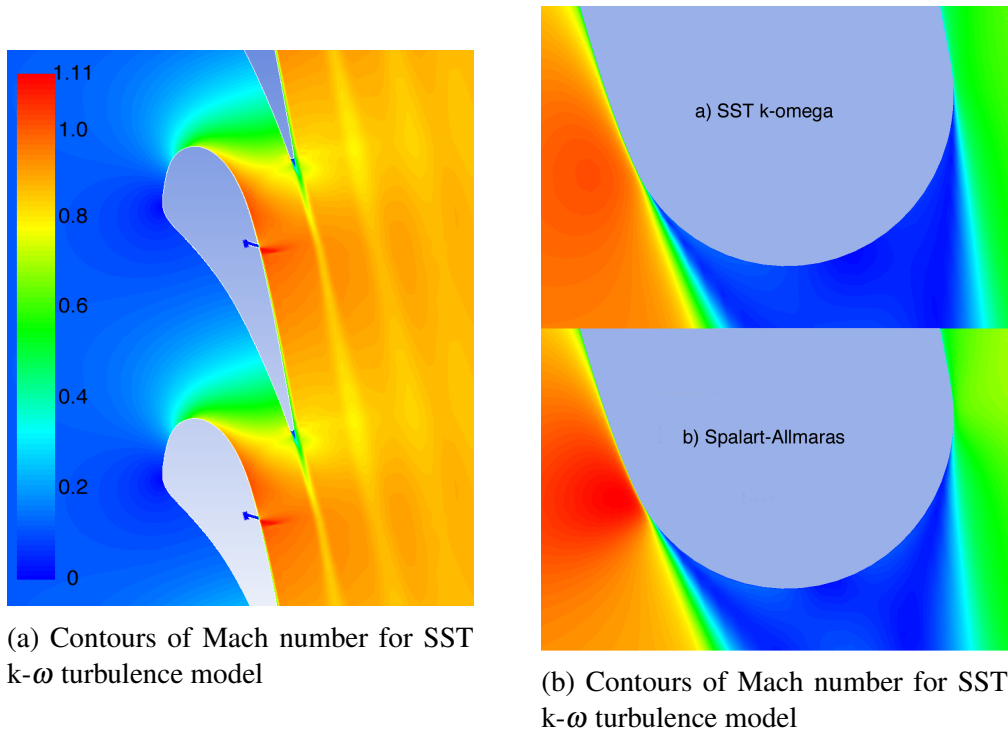


Figure 3.6

Figure 3.6a shows that the simulation has predicted flow turning by the vane, wake regions downstream of the trailing edge, an expansion near the throat, and a weak shock immediately downstream of the cooling hole.

Figures 3.6ba and 3.6bb visualise the *fast patch* at the vane trailing edge. Both show that this region is characterised by flow acceleration and a significant reduction in boundary layer thickness. This flow region is just downstream of the geometric throat so some acceleration is to be expected. Previous computational studies of the Trent XWB 84K HP NGVs [15] predict such behaviour. Checks were undertaken to ensure that the *fast patch* was not the result of a locally inviscid region or some other such computational error.

The local boundary layer thickness in Figure 3.6ba (SST $k-\omega$) is approximately 3 times greater than in Figure 3.6bb (Spalart-Allmaras). The peak Mach numbers were 0.858 and 0.961 respectively. Boundary layer separation occurred sooner with SST $k-\omega$ than with Spalart-Allmaras. This resulted in a thicker base region with SST $k-\omega$ than with Spalart-Allmaras.

3.1.6 Comparison of Spalart-Allmaras and SST $k-\omega$ Turbulence Models

Models

The SST $k-\omega$ turbulence model [13] is an eddy-viscosity model that is suitable for compressible flows and can be used all the way down to the viscous sub-layer. It was chosen for this study because of its relatively good performance in separating regions such as the NGV trailing edge.

The Spalart-Allmaras turbulence model [14] is a one-equation model. It has been used successfully for CFD on HP NGVs [15][16]. As present in ANSYS Fluent, it is adaptable to compressible flows and is usable all the way down to the viscous sub-layer. The model works by solving a transport equation for a viscosity-like variable known as the *Spalart-Allmaras variable*. It was also chosen for this study because of its relatively small computational demands.

Discussion of results

Compared to Spalart-Allmaras, SST $k-\omega$ predicted the following differences in flow features: less acceleration around the convex curve of the pressure-side trailing edge; a thicker boundary layer in this region; and earlier boundary layer separation. These differences would be expected to occur together - the less the flow is allowed to remain attached to a convex curved surface, the smaller the peak velocity should be. The boundary layer thickness ought to increase accordingly.

This suggests that the magnitude of the peak velocity at the *fast patch* depends upon exactly where boundary layer separation occurs at the onset of the base region. A limitation of most RANS CFD solvers is the inability to predict separation with a useful degree of accuracy. The location of the separation point is sensitive to which turbulence model is used. Changing the turbulence model did not significantly affect the computed characteristic between cooling hole position and total engine capacity.

Hambidge [15] simulated the same NGV at greater pressure ratios than this study. At the design pressure ratio his simulation predicted a *fast patch* equivalent to what was observed in this study when using SST $k-\omega$. At higher pressure ratios the *fast patch* was predicted to grow away from the vane surface to form

a clearly defined expansion. This is to be expected considering the behaviour of under-expanded supersonic flows post-throat.

This suggests that the *fast patch* has a physical basis in well-understood adiabatic flow. However, direct comparison to 1D adiabatic nozzle theory is presently not possible for two reasons. Firstly the flow in this case is highly 2D, and secondly the CFD is demonstrated to be inadequate in predicting the 2D flow structures in question.

3.2 Single Film Cooling Row Positioning - Quasi-3D Study

A CFD study was performed to examine how predictions of the effects of single cooling row positioning differ when the circular shape of the cooling hole is accounted for. A quasi-3D geometry was created and meshed to feature a circular cooling hole without introducing further complications such as NGV end-walls or span-wise variation in aerodynamic profile. The effects of 3D mixing downstream of the hole were considered and compared to the accompanying 2D study.

3.2.1 Geometry

This study used the same Trent XWB 84K profile as the 2D single-cooling-hole study. The profile was extruded in the span-wise direction into a thin strip of NGV surface. The cooling hole was modelled as a single cylindrical passageway with a cylindrical plenum and placed in the centre of the thin strip. The width of the strip was such that this geometry could repeat periodically in the span-wise direction to produce an infinitely long cooling row whose hole spacing was engine-representative.

3.2.2 Boundary Conditions

The boundary conditions for this CFD study were the same as those for the accompanying 2D study, except this study introduced an additional periodic boundary to allow the modelling of an infinite span of circular cooling holes. Film cooling blowing ratio was matched between the 2D and 3D simulations. The present quasi-3D study simulated a cooling hole at position 0, the furthest position upstream. This was compared to a case with the same hole position from the accompanying 2D study.

3.2.3 Mesh

The requirement for periodicity in two axes placed strict requirements on the mesh for this study. As a result a fully structured mesh was produced using the ICEM software tool. The mesh used nested o-grids to resolve the interior of the cooling hole. Sufficient resolution of the NGV boundary region (y -plus of 2.5) was achieved without the use of a dedicated o-grid for this region. This was beneficial in meeting the requirement of mesh periodicity in the pitch-wise direction. The resulting mesh had approximately 1.6 million elements. The mesh is shown in Figures 3.7 and 3.8.

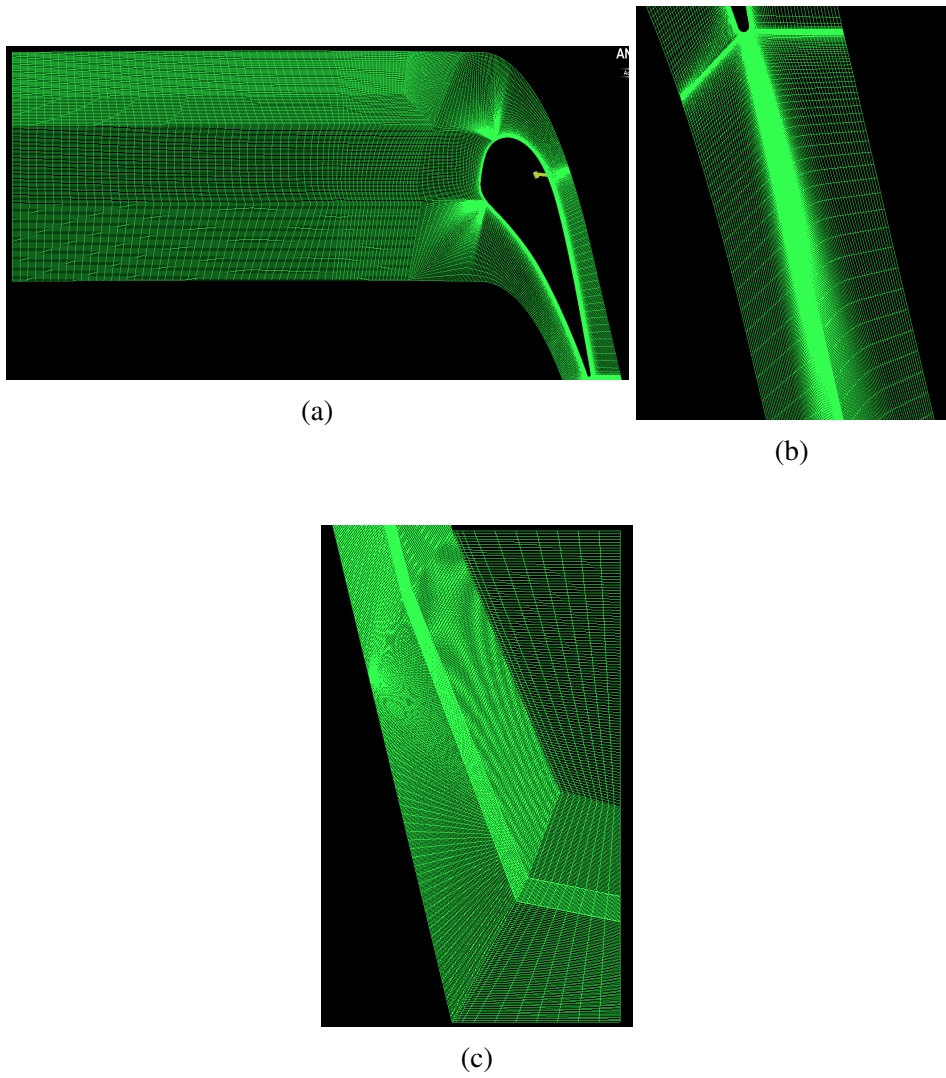


Figure 3.7: Details of mesh for single-cooling-hole quasi-3D study

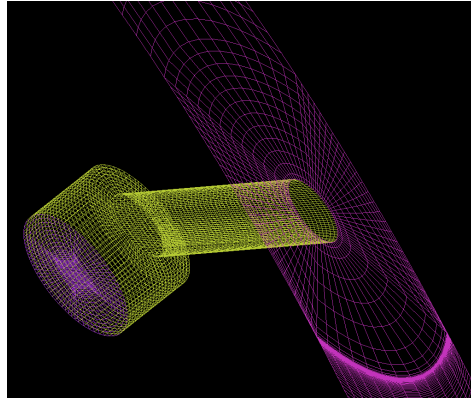


Figure 3.8: Detail of cooling hole mesh for quasi-3D study

3.2.4 Simulation

The quasi-3D simulation was performed in FLUENT using the same script as the accompanying 2D simulations and the parameters from Table 3.1. Overall solution times were approximately 10 days.

3.2.5 Results

Comparison of Mixing in 2D and Quasi-3D

One of the purposes of this study was to evaluate and discuss the significance of 3D mixing effects due to a circular hole compared to a 2D rectangular slot. Mixing in the 3D case would be enhanced by vortices from the interaction of coolant and mainstream. The 2D case does not model this effect, but could have a mixing “advantage” because there are no sections of span into which coolant was not being introduced at full blowing ratio, whereas the 3D case could have sections of span between the holes where coolant is not encountered.

For both 2D and 3D, specific entropy was evaluated at a series of axial planes downstream of the cooling hole. The planes traversed the whole passage. The planes were spaced to intersect the NGV suction-side surface at locations 1 hole diameter apart on the surface. Values of specific entropy were mass-averaged at these planes. The development of entropy downstream of a cooling hole at position 0 is shown in Figure 3.9.

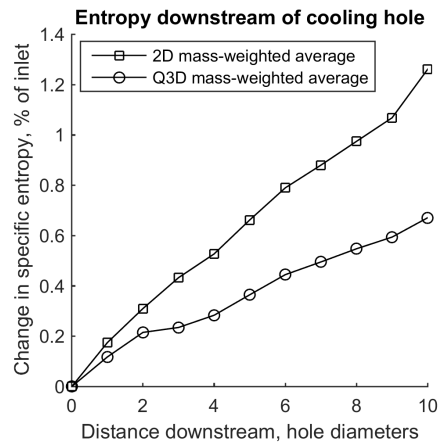


Figure 3.9: Development of entropy downstream of a single suction-side cooling hole, 2D and quasi-3D

Figure 3.9 shows that both the 2D and quasi-3D simulations predicted a linear development of entropy in the mixing region immediately downstream of the single cooling hole. Specific entropy development per unit distance was approximately 2 times greater in 2D than in quasi-3D. This suggests that more mixing occurred in the simulated 2D boundary layer than in the 3D one.

CFD Visualisations

Contours of specific entropy (relative to the inlet mass-weighted average) on the surface of the NGV are shown in Figure 3.10.

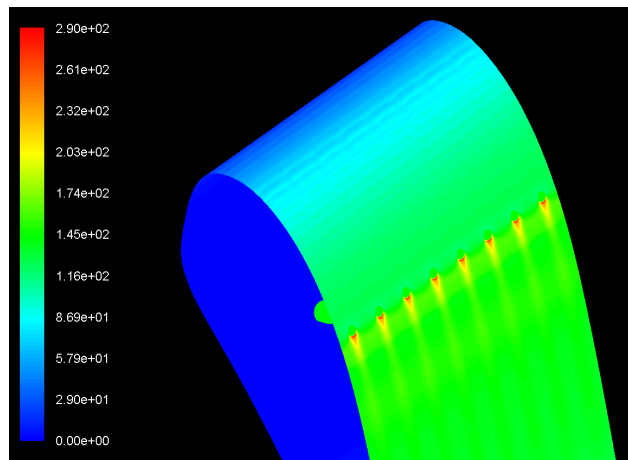
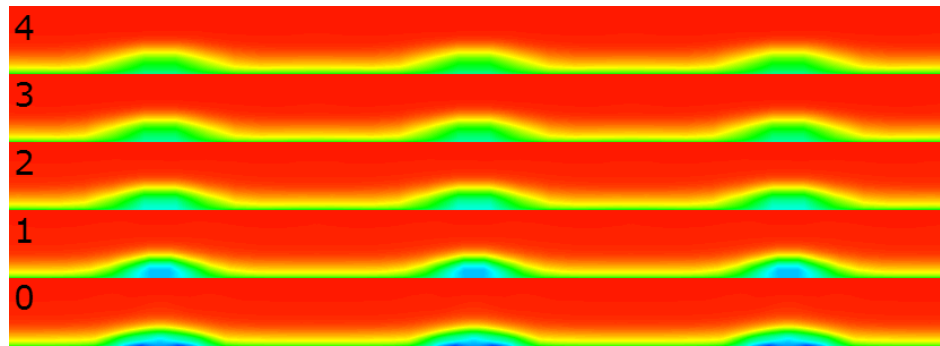


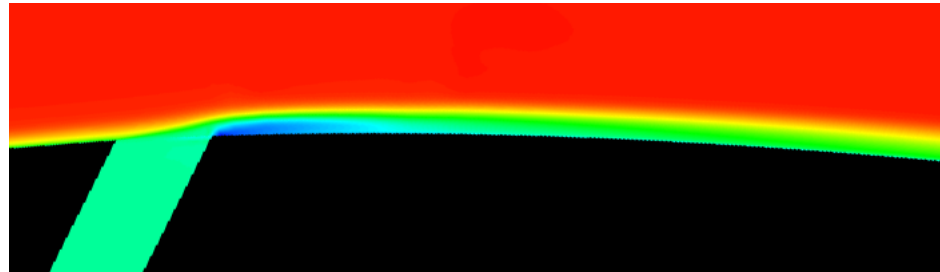
Figure 3.10: NGV surface contours of specific entropy, quasi-3D

figure 3.10 show that there are significant regions of the NGV surface in between the cooling holes where no mixing is occurring adjacent to the NGV surface. This supports the hypothesis that mixing in this case is limited by the relatively small amount of span available for it to occur compared to the case in which effectively all the span is available.

Contours of total pressure on planes in the flow are shown in Figure 3.11.



(a) Contours of total pressure in traverse planes normal to NGV surface, labelled by distance downstream of single cooling hole in hole diameters



(b) Contours of total pressure in plane intersecting the single cooling hole

Figure 3.11

Figure 3.11 illustrates 2 features of film cooling hole flow that are not captured by the accompanying 2D study. Firstly the presence of a separation bubble downstream of the cooling hole is clearly observable. The bubble has a maximum height of approximately 1/5 of a hole diameter, and it dissipates approximately 2.5 hole diameters downstream.

Figure 3.11 also further supports the hypothesis that coolant/mainstream mixing is limited because areas in between the cooling holes never encounter the coolant.

Discussion of Results

With the aim of examining differences between a study of a single suction-side cooling hole in 2D and the same study in 3D, several conclusions can be drawn. It has been found that coolant/mainstream mixing differs significantly between the 2, but the result may be counter-intuitive: when blowing ratios were matched between 2D and 3D, the 2D case experienced more entropy production downstream of the cooling hole compared to the 3D case. This is concluded to be because the 3D case deprives large areas of span of coolant, preventing any mixing in these areas. This may also be considered reasonable by saying that the amount of coolant delivered per unit span in the 3D case is less than 1/2 what it is in the 2D case. This poses the question of whether matching blowing ratio is the best way to compare film cooling CFD between 2D and 3D. In general it may still be concluded that significant differences exist in the modelling of coolant/mainstream mixing between 2D and 3D.

3.3 2D Capacity of Scanned Trent 900 NGVs Without Cooling Features

3D CFD predictions of Trent 900 NGV capacity characteristics have been made by Rolls-Royce [16][17]. The present study has made 2D CFD predictions using the same NGV geometries as the Rolls-Royce 3D study. The 3D and 2D results were compared.

3.3.1 Geometry

Several standards of Trent 900 NGVs have been produced. Two standards were considered by Rolls-Royce in their 3D CFD studies [16][17]. They are referred to as the M-skew standard and the EP1 standard. Rolls-Royce randomly selected three production NGVs from each standard and measured their surface geometries using the *white light/GOM* scanning method. This resulted in the geometric definition files which were used by this study. These files do not include film cooling holes or the trailing edge slot. The trailing edges are smoothly rounded.

The files were processed into 2D geometries using the method described in Section 3.1.1. This resulted in 6 different 2D NGV profiles.

Rolls-Royce computed the geometric throat areas of the 6 vanes using the scanned data. The vanes and their geometric throat areas are listed by serial number in Table 3.2.

Table 3.2: Trent 900 scanned vanes

Production Standard	Serial Number	Throat Area (mm ²)
M-skewed	KSZ03	1578.4
	KTA01	1584.6
	KVD04	1571.4
M EP1	PNN06	1592.0
	PNS03	1587.2
	PNS04	1598.8

The NGV profiles were placed in computational domains similar to those described in Section 3.1.1. Domain outlet sections were inclined at the NGV turning angle and NGV spacing was engine-representative.

3.3.2 Boundary Conditions

Boundary conditions were the same as those described in Section 3.1.2 and illustrated in Figure 3.2a. Periodic spacing was representative of the Trent 900.

3.3.3 Mesh

A mesh was made using the same methodology as described in Section 3.1.3. Overall cell count was reduced because no cooling hole meshing was present. The mesh is shown in Figure 3.12.

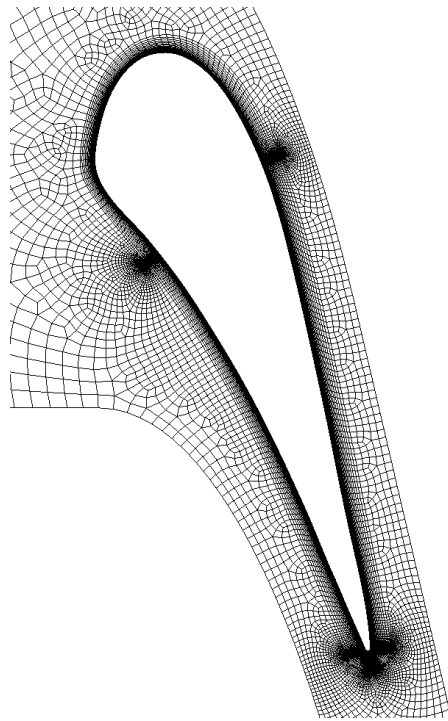


Figure 3.12: Mesh for Trent 900 smooth-vane capacity study

3.3.4 Simulation

Simulations were performed in FLUENT using *Journal* scripts similar to those described in Section 3.1.4. FMG initialisation was used. Solutions were then converged at incrementally increasing pressure ratios between 1.01 and 3.33. Capacity data were saved after each increment. There were 32 increments and typical overall solution times were approximately 10 hours.

Solutions were computed using the SST $k-\omega$ turbulence model.

Simulation parameters are given in Table 3.3.

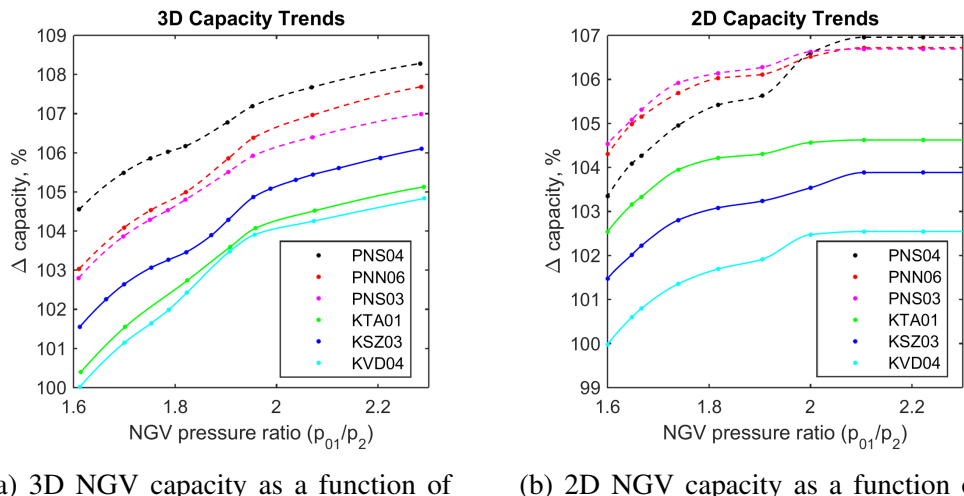
Table 3.3: Simulation Parameters

Parameter	Value
NGV turning (degrees)	76.891
Design pressure ratio	1.79
Inlet total pressure (Pa)	4.3256×10^6
Inlet total temperature (K)	300
Outlet static pressure (design) (Pa)	2.4156×10^6
Outlet static temperature (Pa)	300
Solver type	Density-based
Cell count	35,000

3.3.5 Results

NGV Capacities as a Function of Pressure Ratio

Rolls-Royce's 3D NGV capacity is plotted as a function of NGV pressure ratio in Figure 3.13a. 2D NGV capacity is plotted as a function of NGV pressure ratio in Figure 3.13b.



(a) 3D NGV capacity as a function of pressure ratio for 6 vanes

(b) 2D NGV capacity as a function of pressure ratio for 6 vanes

Figure 3.13

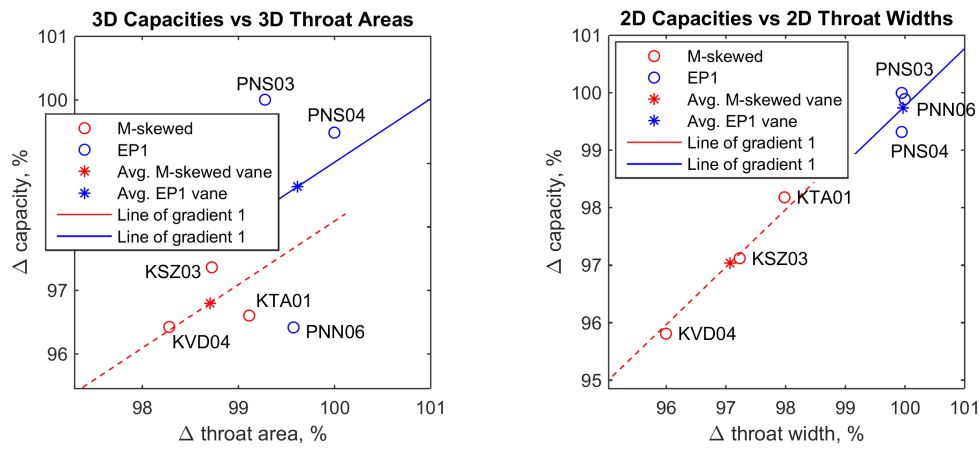
Figure 3.13b shows that the predicted 2D capacity of all six NGVs increased with pressure ratio. All six vanes were fully choked above approximately $PR =$

2.1. All six capacity characteristics demonstrated a non-smooth region around $PR = 1.9$. This behaviour has been observed in previous 2D and 3D CFD and testing [1][2][15][16].

Capacity as a Function of 2D Throat Area

Rolls-Royce compared the predicted 3D capacities of the 6 NGVs at design pressure ratio. The capacities of the 6 NGVs were compared as a function of their throat areas. Predictions of 3D throat area were made using the 3D STL files from the company's *white light/GOM* scanning method [16]. 3D capacity is plotted as a function of 3D throat area in Figure 3.14a.

The present study compared the predicted 2D capacities in the same way. 2D throat area was predicted using a MATLAB code that calculated the shortest distance between two adjacent vanes. The inputs to this MATLAB code were the 2D geometries described in Section 3.3.1. 2D capacity is plotted as a function of 2D throat area in Figure 3.14b.



(a) 3D NGV capacity percentage delta as a function of 3D throat area for 6 vanes

(b) 2D NGV capacity percentage delta as a function of 2D throat area for 6 vanes

Figure 3.14

Comparison of 2D Mach 1 Contours for the 6 Scanned Vanes

The 2D CFD solutions for the 6 scanned Trent 900 NGVs were analysed to visualise the Mach 1 contour for each. These are shown in Figure 3.15.

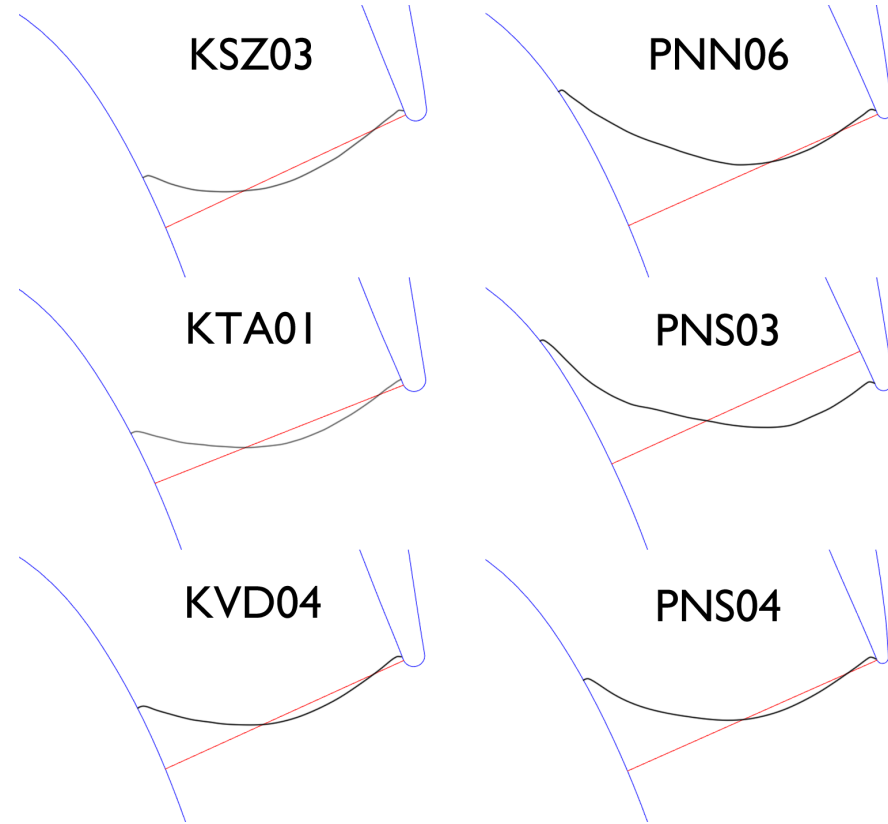


Figure 3.15: Mach 1 contours for 6 scanned Trent 900 NGVs

Figure 3.14b shows that within the M-skewed standard, variation in capacity was almost linear with throat area. Figure 3.15 shows that Variation in Mach 1 contours within the M-skewed standard was minimal. This comparison suggests that aerodynamic differences were minimal within M-skewed, and that capacity changes were driven by area changes.

In contrast, Figure 3.14b shows that within the EP1 standard, throat width did not vary significantly but capacity did. Figure 3.15 shows that variation in Mach 1 contours within the EP1 standard was significant. This comparison suggests that capacity changes within EP1 were driven by aerodynamic differences.

Comparison of 2D Results with Prior 3D Data

The 2D characteristics in Figure 3.13b differ from the 3D characteristics in Figure 3.13a with respect to choking. This is because they did not account for spanwise variations in pressure ratio that occur in the 3D case. These span-wise variations delay the onset of stalling in 3D CFD and in physical cases, compared to 2D CFD.

Suppose the 6 vanes were listed in order of capacity at some pressure ratio. For all pressure ratios, this order would be different between Figure 3.13a and Figure 3.13b. This shows that comparing the 3D capacity of some vanes is not a predictor of comparing the 2D capacity of the same vanes. The converse is also true.

If aerodynamic differences are minimal among a number of NGVs, it is expected that the relationship between percentage change in capacity and throat area will be linear with gradient 1 [18][19]. Any scatter from this *area line* indicates that significant aerodynamic variations exist between the group of NGVs. It was hypothesised that aerodynamic differences are minimal between the three vanes of each standard (M-skewed and EP1). Any such differences would be the result of manufacturing variation.

In Figures 3.14a and 3.14b, *area lines* have been plotted (1% throat area for 1% capacity). Extra points have been plotted at the mean throat area and mean capacity for each vane standard. The lines intersect the mean points.

Figure 3.14a shows complete scatter from the *area lines* for both standards. No correlations appear between capacity and throat area. Any such effect is not discernible among aerodynamic variations. Figure 3.14b shows significantly less scatter for both standards. The capacities of the M-skewed standard appear to correlate strongly with their throat areas. No such correlation is apparent for the EP1 standard. Point PNS04 may be an outlier.

The hypothesis of minimal aerodynamic differences is rejected in the case of 3D capacity, and confirmed in the case of 2D capacity. This suggests that there are significant NGV aerodynamic effects that act in 3D but not in 2D. These effects may be the result of vane loading variations that are not captured by examining the mid-span. They may also be the result of span-wise variations in trailing edge thickness. Such variations could exist even though the trailing edges have been rounded.

3.4 Effects of Trailing Edge Design on Capacity

Computational and experimental studies [6][7][8][9] have demonstrated that there may be significant reductions in loss using an NGV with a coolant slot positioned in the centre of the trailing edge, rather than off-set to one side. CFD was used to simulate a novel NGV having a rounded trailing edge with a centrally positioned coolant ejection slot. Variations were made to the size of the pressure-side lip of this novel geometry and capacity predictions were made.

CFD was also used to simulate a geometry resembling a production NGV with a realistic trailing edge. Variations were made to the size of the suction-side lip of this realistic geometry and capacity predictions made. Unsteady simulations

were performed on 2 of the realistic trailing-edge geometries and the results compared with steady-state simulations. For the case of an unmodified realistic NGV at design conditions, visualisations were made of the periodic vortex shedding downstream of the NGV trailing edge. Periodic variation of static pressure on the vane surface was predicted and plotted.

Comparisons are made between the results of the pressure-side cutback case and the suction-side cutback case.

3.4.1 Pressure-Side Cutback Geometry

The base-line geometry for the pressure-side cutback study was scanned vane KSZ03 from the M-skewed standard of Trent 900 NGVs (see Table 3.2). The 2D mid-span profile was defined as in Section 3.1.1.

For the pressure-side cutback study, the trailing edge of the baseline profile was changed to a novel design by cutting back approximately 2.6% of chord and defining a straight rectangular cooling slot whose length was approximately 15% of chord. These dimensions were chosen so the smallest wall thickness would exceed the smallest wall thickness of the real vanes measured in Rolls-Royce's report [16]. The centred-ejection geometry is shown in Figure 3.16.

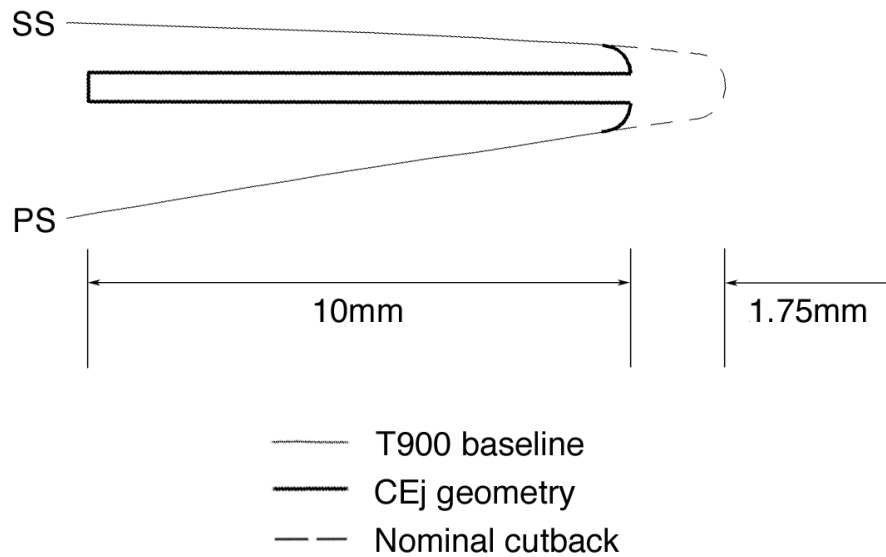


Figure 3.16: Design of Trent 900 centred-ejection geometry

A MATLAB script was used to produce versions of the pressure-side cutback geometry with incremental cut-backs from the pressure-side lip of the slot. In each

case the blending radius at the slot edge was increased accordingly. Pressure-side cut-back size was parametrised by *cutback ratio* r_{cp} , where

$$r_{cp} = \frac{\text{cutback length}}{\text{cooling slot width}} \quad (3.5)$$

Examples of these cut-backs are shown in Figure 3.17.

$r_{cp} = 0, 1, 2, 3$ are labelled.

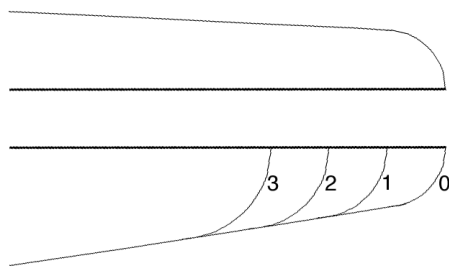


Figure 3.17: Trailing-edge cut-back scheme, r_{cp} values given

3.4.2 Suction-Side Cutback Geometry

The base-line geometry for the suction-side cutback study was scanned vane KSZ03 from the M-skewed standard of Trent 900 NGVs (see Table 3.2). The 2D mid-span profile was defined as in Section 3.1.1.

For the suction-side cutback study, the geometry was intended to be a mid-span section of scanned vane KSZ03. Dimensions were derived from the measurements of the scanned vane given in Rolls-Royce's report [16]. The trailing-edge shape described in the report was altered for the purposes of this study in the following ways: the curved surface on the inside of the pressure-side lip was changed to a straight line with an angular corner, and the curved tip of the suction-side lip was changed to a square end. These changes and the resulting geometry are shown in Figure 3.18.

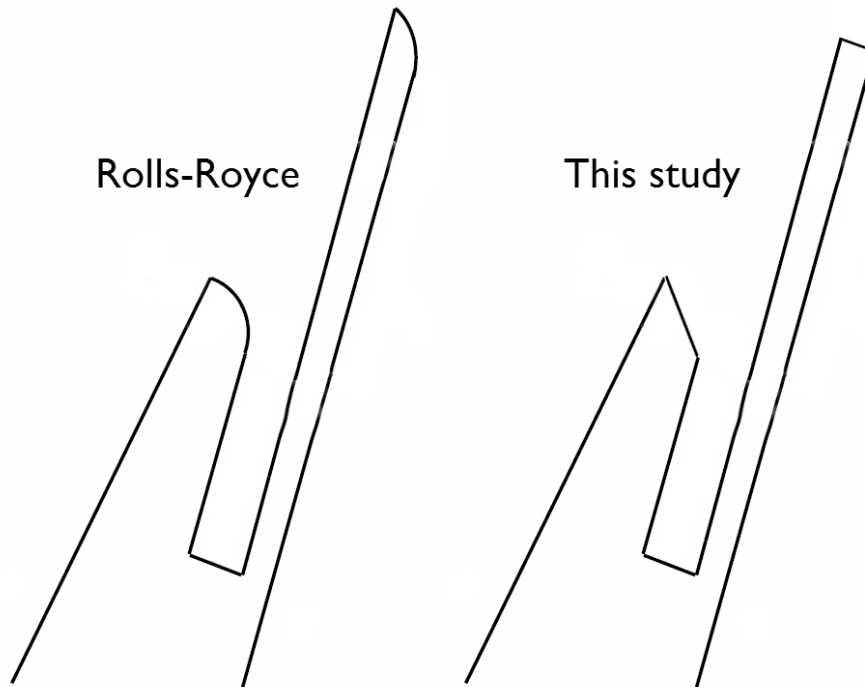


Figure 3.18: Changes to Rolls-Royce trailing-edge geometry for this study

These changes were made from the Rolls-Royce definition of geometry because 1) it facilitated meshing and 2) close inspection of physical NGVs reveals that their actual shape is closer to that of the changed geometry than it is to that previously defined - real NGVs have corners rather than smooth curves in the places in question, because of their manufacturing process.

The suction-side cutback study used a MATLAB script to produce versions of the geometry with incremental cutbacks from the suction-side lip of the slot. This process was designed to simulate an incremental removal of material from this part of a real NGV. The regime of simulated cutbacks was between the baseline NGV and the case of no remaining suction-side lip. This regime was divided into 10 increments which are referred to here as the cutback sizes for the suction-side cutback study. Hence in this scheme $r_{cs} = 0$ is the unmodified NGV and $r_{cp} = 10$ is a fully removed suction-side lip. The cutback scheme is illustrated in Figure 3.19.

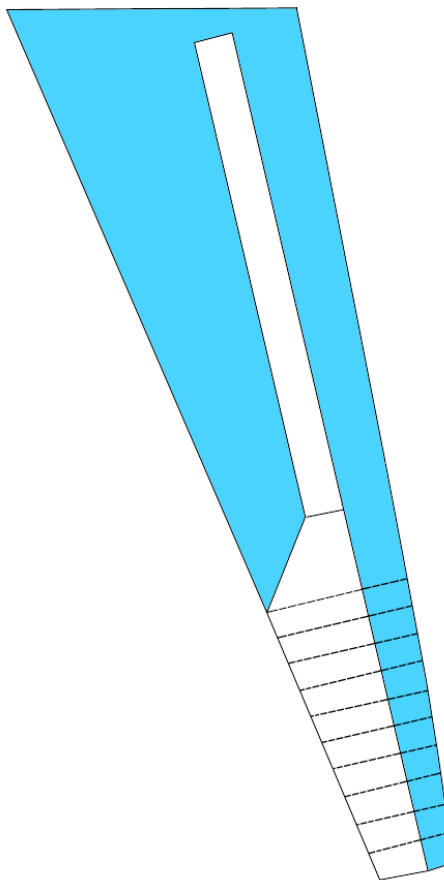


Figure 3.19: Cutback scheme for suction-side study

3.4.3 Boundary Conditions and Steady-State Simulation

Overall boundary conditions were the same as those described in Section 3.1.2 and illustrated in Figure 3.2a. Periodic spacing was representative of the Trent 900. The inner end of the cooling slot was set as an inlet. Its mass flow rate was set as 3% of mainstream at design pressure ratio. The simulation procedure was the same as in Section 3.3.4.

3.4.4 Pressure-Side Cutback Mesh

This mesh was based on that used for Trent 900 smooth vanes as described in Section 3.3.3. A meshing scheme was designed to maximise consistency between simulations of varying cutback size. For the case of centred ejection with zero cutback, 1 structured block was added to the baseline mesh. For cases with cutbacks, 2 structured blocks were added to the baseline mesh. The NGV mesh for $r_{cp} = 0$

is shown in Figure 3.20. Trailing-edge meshes for $r_{cp} = 0, 1, 2, 3$ are shown in Figure 3.21.

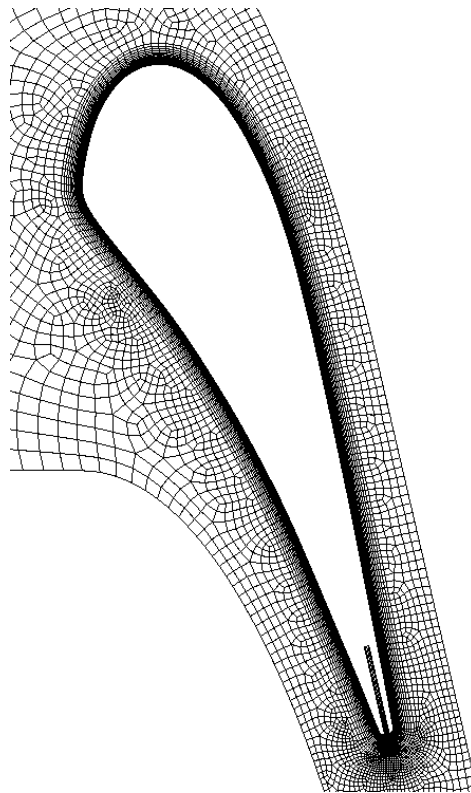


Figure 3.20: NGV mesh for centred-ejection study

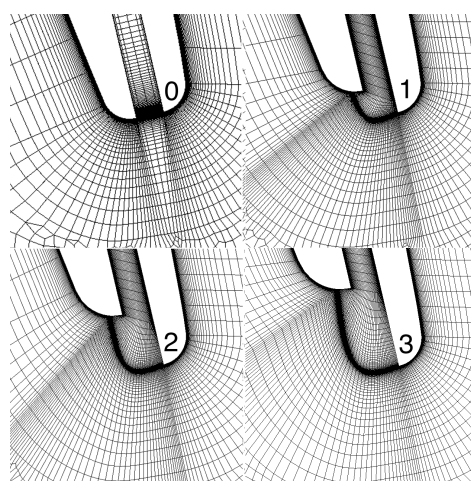


Figure 3.21: Trailing-edge meshes for centred-ejection study, r_{cp} values given

3.4.5 Suction-Side Cutback Mesh

This mesh was designed so that removed sections of the vane were replaced with regions of structured mesh as the cutbacks progressed. This allowed the other mesh regions to remain unchanged between different cutbacks. This scheme involved dividing the regions around the trailing edge into several structured quadrilateral blocks. Outside of these was a structured o-mesh surrounding the whole vane for boundary layer resolution with an unstructured far-field, as in Section 3.3.3. An example of the suction-side cutback mesh is shown in Figure 3.22. The region of removed material replaced by structured mesh is visible.

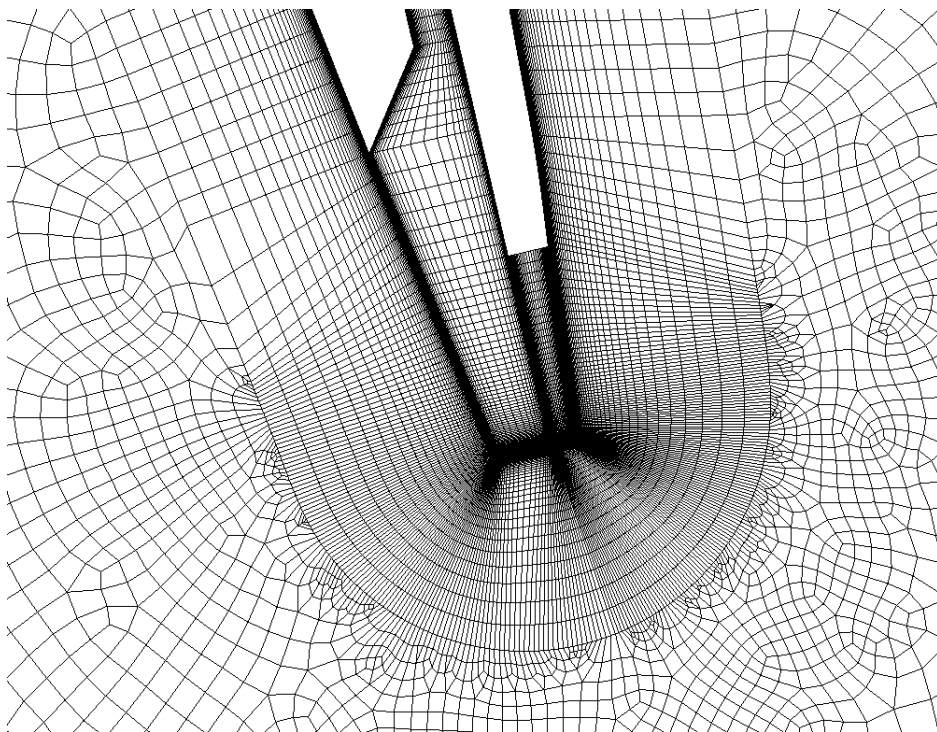


Figure 3.22: NGV mesh for suction-side cutback study

3.4.6 Unsteady Simulation and Mesh Modification

Ansys FLUENT was used to perform unsteady transient simulations of two of the realistic suction-side cutback geometries: the case of no modification, and the case of a fully removed suction-side lip. The solver and models were the same as the steady-state simulations. The time-step was $5 \times 10^{-7}s$.

Unsteady Capacity Predictions

The mesh used for unsteady capacity predictions was the same as in the steady-state simulations. Pressure ratio was varied and capacity predicted at each pressure ratio to produce capacity characteristics. The simulation procedure was designed to converge a steady-state solution at each pressure ratio, then simulate 1000 time-steps.

Resolution of Periodic Vortex Shedding

An unsteady solution was produced for the case of an unmodified NGV with a realistic trailing edge. The existing mesh was refined significantly in order to give more resolution of vortex shedding at the vane trailing edge. y -plus decreased from approximately 2.5 to less than 1. Cell count increased from approximately 40,000 to approximately 400,000. The general meshing strategy was unchanged.

A steady solution was converged at the design pressure ratio of 1.79. This was then subject to 20,000 time-steps, a total simulation time of 0.01s. A value for static pressure in the base region of the NGV suction-side lip was saved after each time-step.

3.4.7 Blowing Rate Variation

A study was conducted into the effect of varying trailing edge coolant blowing rate on loss. Loss was defined according to Raffel and Kost [10] (see Section 2.2). Trailing edge coolant mass flow rate was specified at the inlet to the slot plenum and varied between 0% and 4% of mainstream in increments of 0.5%.

3.4.8 Results

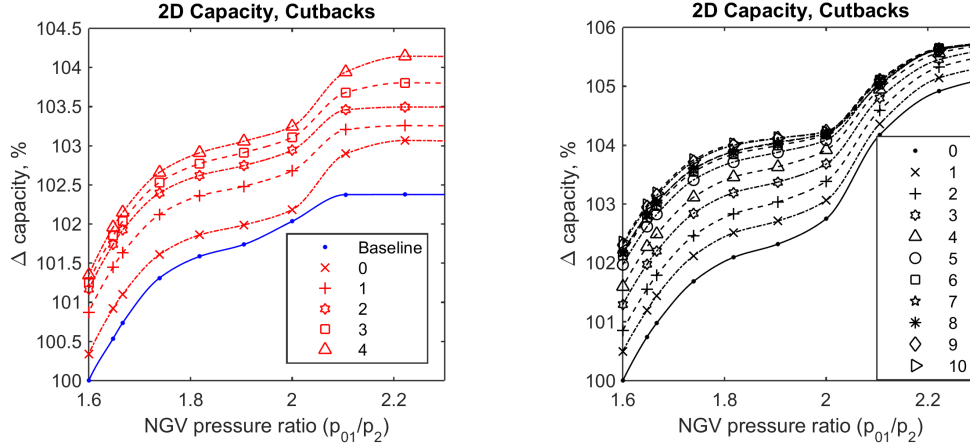
Capacity Trends with Varying Pressure-Side Cutback Size

Capacity was plotted as a function of pressure ratio for the set of pressure-side cutback geometries. These trends are plotted for cutbacks 0-4 in Figure 3.23a. The trend for the baseline NGV is included.

Figure 3.23a shows that all centred-ejection designs increased capacity compared to the baseline. The shape of the capacity trend was significantly different between the baseline and $r_{cp} = 0$. The shape was also significantly different between $r_{cp} = 0$ and cutback $r_{cp} = 1$. There was an approximately monotonic change between $r_{cp} = 1, 2, 3, 4$.

Capacity Trends with Varying Suction-Side Cutback Size

Inlet capacity Γ_{tota} was plotted as a function of pressure ratio for the set of suction-side cutback geometries. These trends are plotted for the full range of cutbacks in Figure 3.23b.



(a) 2D NGV capacity as a function of pressure ratio for baseline and pressure-side cutback trailing edge geometries, r_{c1} values labelled

(b) 2D NGV capacity as a function of pressure ratio for suction-side cutback trailing edge geometries, r_{cs} values labelled

Figure 3.23

Figure 3.23b shows that capacity increased almost monotonically with increasing suction-side cutbacks. All capacity trends were similar in shape. The increase in capacity with r_{cs} was smaller at higher r_{cs} .

Loss as a Function of Suction-Side Cutback Size

Energy loss (as defined by Raffel and Kost [10]) was calculated from the CFD solutions for varying suction-side cutbacks at the design pressure ratio of 1.79. Total and static pressure values were integrated along the length of the CFD domain exit plane. The integrated values were used to calculate energy loss.

Energy loss is plotted as a function of suction-side cutback r_{cs} in Figure 3.24.

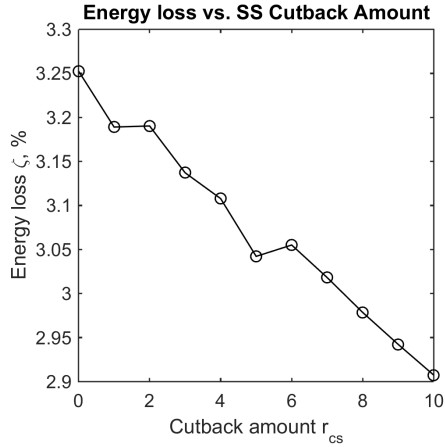


Figure 3.24: Energy loss as a function of suction-side cutback r_{cs}

Figure 3.24 shows that energy loss not accounting for coolant energy decreased approximately linearly as r_{cs} decreased with increasing cutbacks. This result supports the hypothesis that trailing edges with centred ejection are capable of producing less loss than those with a suction-side lip, despite the base region of the NGV having a larger area. In the present case, it is concluded that progressively removing sections of the suction-side lip equates to moving closer to a centred-ejection design having decreased loss.

CFD Visualisations for Pressure-Side Cutbacks

Contours of Mach number are shown in Figure 3.25 for varying pressure-side cutbacks at $PR = 1.79$ (design) and 3.33 (fully choked). $r_{cp} = 0, 1, 2, 3$ are shown.

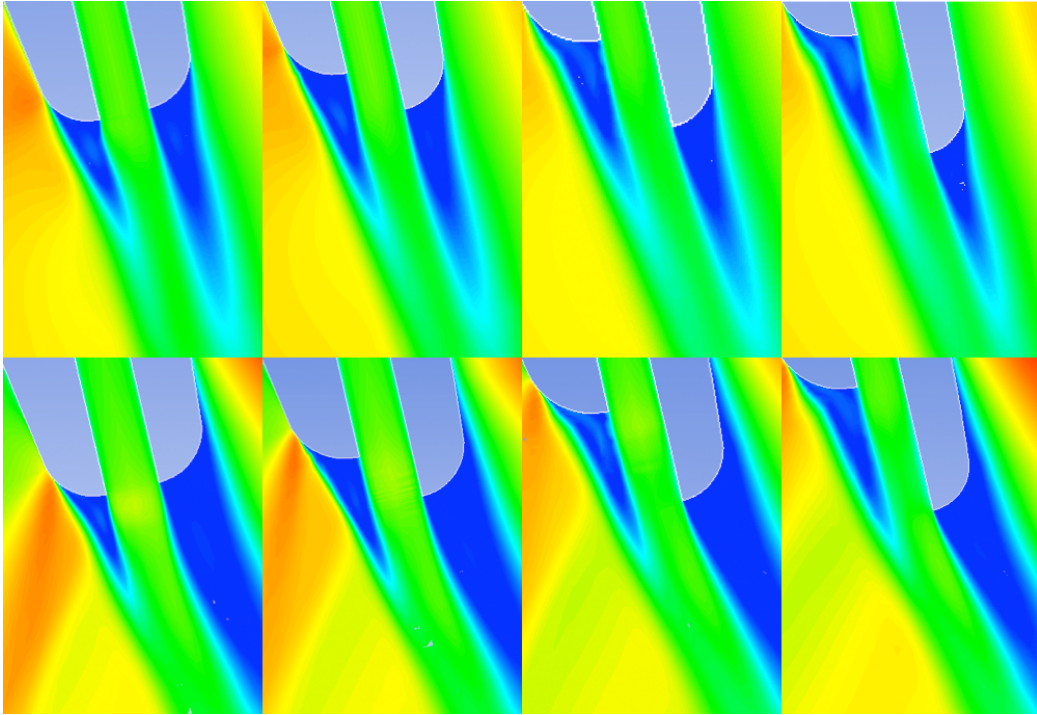


Figure 3.25: Contours of Mach number for $r_{cp} = 0, 1, 2, 3$ and $PR = 1.79, 3.33$

Figure 3.25 shows that, in all cases, separated wake regions were present downstream of the 2 trailing-edge lips. As r_{cp} increased, the thickness of the pressure-side lip increased. This caused the size of the pressure-side wake to increase. Future studies should determine whether this causes an increase in loss.

There was a post-throat expansion which was fully formed at $PR = 3.33$. As r_{cp} increased, the expansion moved upstream with the pressure-side lip. The sonic throat moved into regions of increasing geometric throat area. This suggests that the observed relationship between r_{cp} and Γ may be governed by the effective area of the sonic throat.

Figure 3.25 also shows that the novel NGV was not achieving the design amount of flow turning. The trailing-edge slot was aligned with the design flow exit angle. At $PR = 3.33$ the exit flow was angled away from the slot by approximately 20° . This suggests that the removal of 2.6% of chord from the baseline NGV has significantly affected its aerodynamics.

CFD Visualisations for Suction-Side Cutbacks

Contours of Mach number are shown in Figure 3.26 for varying suction-side cutbacks at $PR = 1.79$ (design). $r_{cs} = 0, 2, 4, 6, 8, 10$ are shown.

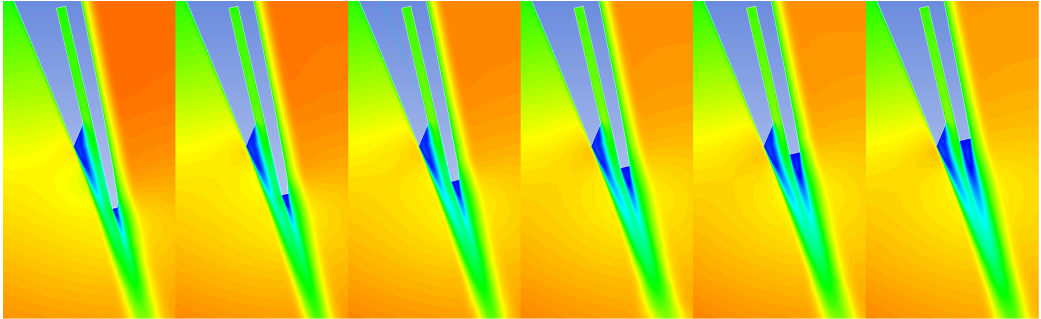


Figure 3.26: Contours of Mach number for $r_{cs} = 0, 2, 4, 6, 8, 10$ and $PR = 1.79$

Figure 3.26 shows that separated wake regions were present downstream of the 2 trailing-edge lips. The most significant change occurring with increasing cutbacks was an increase in the thickness of the suction-side lip with a corresponding increase in the size of the suction-side wake. This is to be expected to correspond to an increase in downstream total-pressure loss with increasing cutbacks.

The flow on the pressure-side of the vane was largely unaffected by increasing cutbacks. This is in agreement with the high degree of similarity between the capacity trends for different values of r_{cs} , suggesting that the cutbacks were not significantly altering the overall aerodynamics of the vane. However, the changes must by definition be aerodynamic, since they are not a result of changing throat area.

Comparison of Pressure-Side and Suction-Side Cutback Results

A MATLAB code was made to evaluate the changes in throat area resulting from pressure-side cutbacks. This code worked in the same way as that described in Section 3.3.5, by finding the shortest distance between the suction side of one vane and the cusp of the pressure-side lip of the other vane. A series of minimum area lines thus produced are shown in Figure 3.27a. Throat area is plotted as a function of r_{cp} in Figure 3.27b.

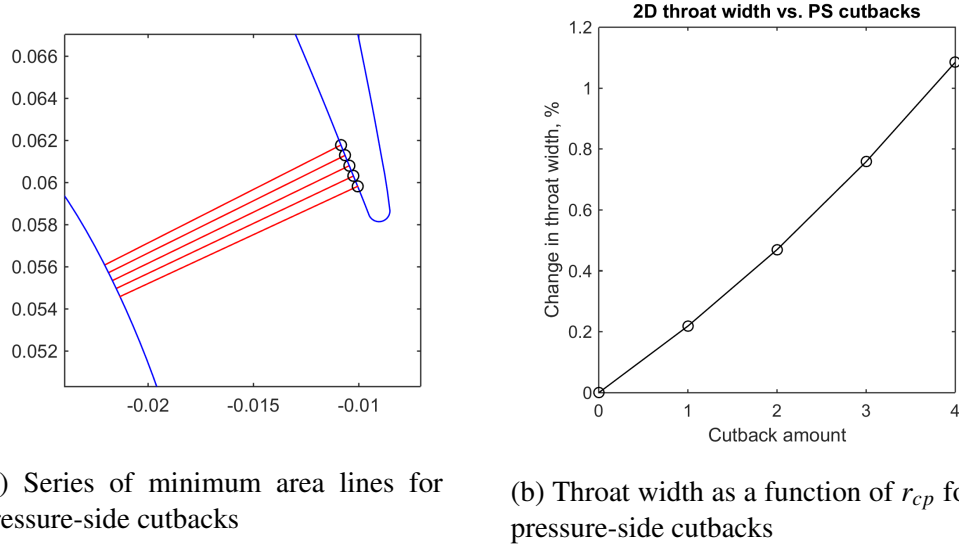
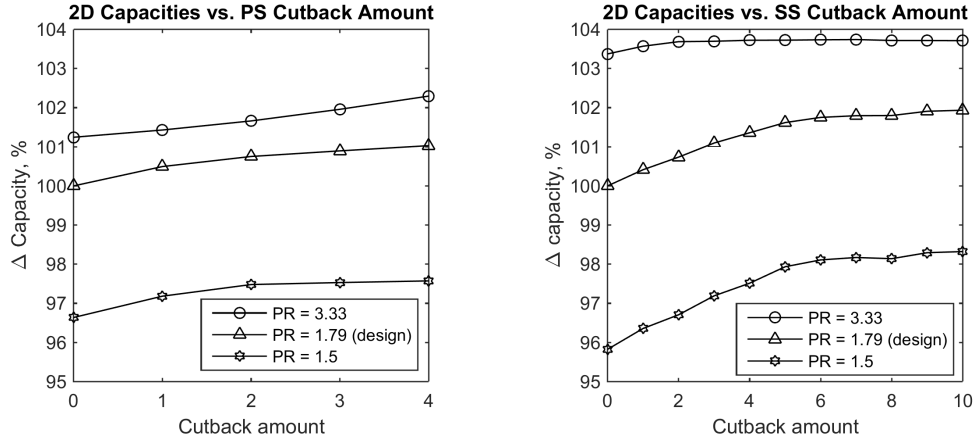


Figure 3.27

Figure 3.27a shows that geometric throat width increased approximately linearly with pressure-side cutbacks. Over the range studied the total delta in area was approximately 1.1%. This suggests that the capacity changes observed with pressure-side cutbacks most likely involve area changes to a significant extent.

Figures 3.28a and 3.28b plot capacity against cutback sizings at 3 different pressure ratios for pressure-side and suction side cutbacks respectively. They show that the sensitivity of capacity to pressure-side cutbacks was greater at higher pressure ratios, but sensitivity of capacity to suction-side cutbacks was greater at lower pressure ratios. It is assumed that throat area is a limiting factor on capacity when the pressure ratio is high enough that the flow is supersonic. This suggests that the mechanism behind pressure-side sensitivity largely involves throat area changes that have a greater effect at higher speeds, but the mechanism behind suction-side sensitivity largely involves aerodynamic changes that have a greater effect at lower speeds.

This conclusion has implications for the broader goal of designing future aero engines with greater robustness of their capacity characteristics. Future designs are to operate at significantly lower NGV pressure ratios. If they have NGV trailing-edge designs similar to those studied here, they will suffer in-service erosion of the suction-side lip, as is the case with existing engines. At lower pressure ratios this could potentially increase NGV capacity and reduce engine efficiency over part of its lifetime. This could be avoided through the use of NGV designs with centred-ejection and hence no suction-side lip.



(a) Capacity as a function of r_{cp} for pressure-side cutbacks

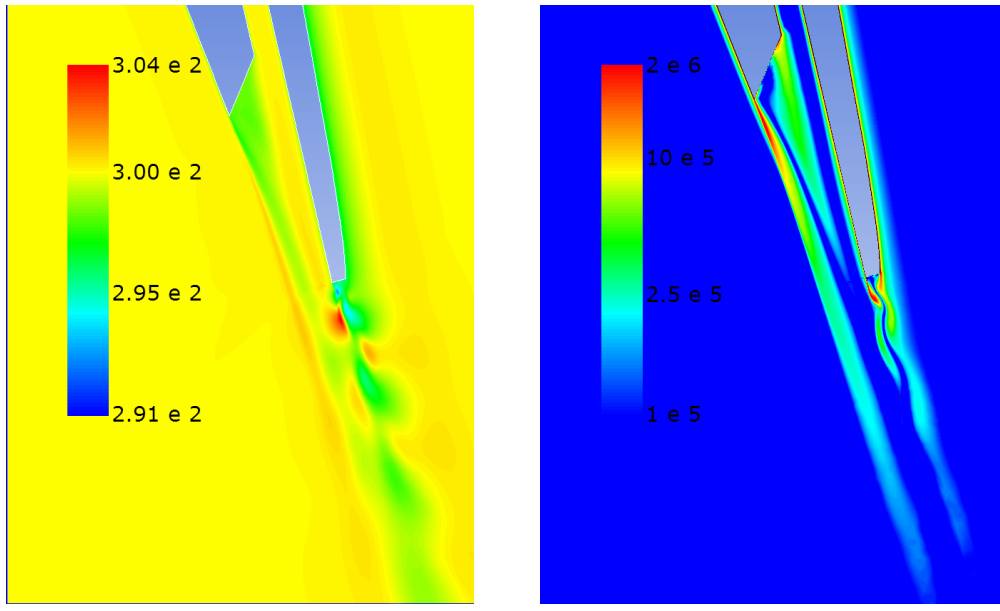
(b) Capacity as a function of r_{cs} for suction-side cutbacks

Figure 3.28

Unsteady Results

Capacity characteristics produced by the unsteady simulations were practically identical to those made by the steady-state simulations. This suggests that unsteady effects do not significantly affect capacity.

Vortex shedding was partially visualised using the refined mesh for a realistic NGV after 20,000 time-steps. Contours of total temperature and vorticity magnitude are shown in Figures 3.29a and 3.29b respectively.



(a) Contours of total temperature showing periodic vortex shedding at the NGV trailing edge

(b) Contours of vorticity magnitude showing periodic vortex shedding at the NGV trailing edge

Figure 3.29

Figures 3.29a and 3.29b show that the first few vortex structures were resolved by the simulation. The remainder of the vortex street was not resolved. This is most likely the result of the downstream mesh being unrefined. It is recognised that, given relatively low levels of mesh refinement, URANS solvers are unable to resolve vortex structures once they have decayed past a certain size [20].

Static pressure at the vane TE measurement location displayed two fundamental variations in time: approximate sinusoids at 100kHz and 200kHz. Figure 3.30 shows a section of the static pressure history.

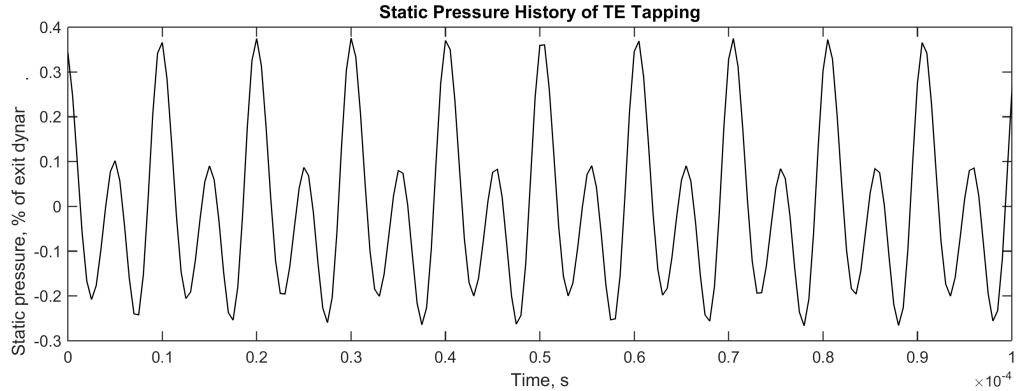
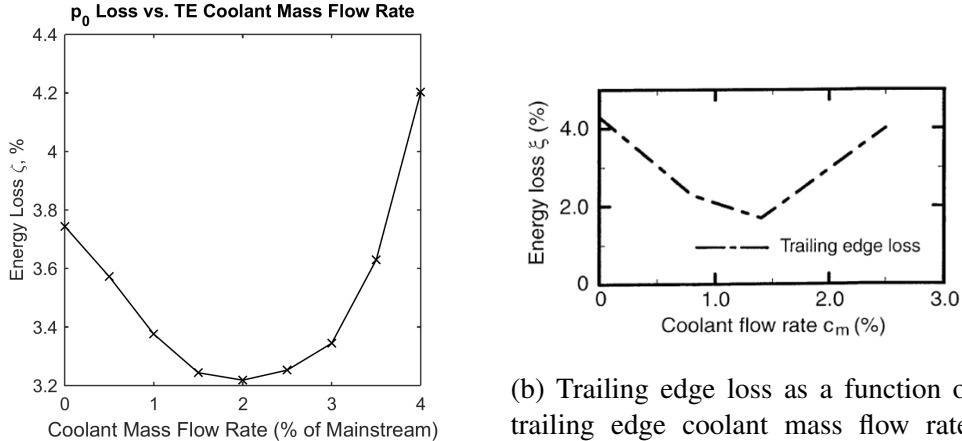


Figure 3.30: Filtered history of integrated static pressure on the vane surface in unsteady simulation

Figure 3.30 shows that the regular periodic oscillations associated with vortex shedding were clearly present at frequencies of 100 kHz and 200 kHz. This may be compared to the vortex shedding frequency of Laskowski and Felten [21]. They predicted approximately 60 kHz with a trailing edge thickness of 1.7 mm. This study's 100 kHz was with a 1 mm thick trailing edge. The two studies are in good agreement since Strouhal frequency scales inversely with characteristic length [22].

Loss as a Function of Trailing Edge Coolant Mass Flow Rate

Energy loss (as formulated by Raffel and Kost [10]) was area-averaged at the domain outlet. This is shown as a function of trailing edge coolant mass flow rate in Figure 3.31a. The equivalent result by Raffel and Kost is shown in Figure 3.31b.



(a) Trailing edge loss as a function of trailing edge coolant mass flow rate, this study

(b) Trailing edge loss as a function of trailing edge coolant mass flow rate, Raffel and Kost

Figure 3.31

Both studies predict the existence of an amount of trailing edge blowing for which loss is minimal. Differences in the magnitude of energy loss variation and optimum blowing rate are explicable by different geometries - Raffel and Kost experimented with a flat plate rig whereas this is 2D CFD on an NGV.

3.5 Conclusions

CFD simulations have been performed to predict how a number of factors affect capacity. These factors may be divided into two categories: those inherent in design; and those inherent in manufacturing, measurement or prediction.

Design effects included 1) the position of a single row of film cooling holes on the suction side; 2) the length of a pressure-side trailing-edge cutback; and 3) the length of a suction-side trailing-edge cutback. It has been predicted that capacity increases when the film coolant is injected into regions further downstream having slower flow. The precise local flow speed metric is likely to reflect a combination of surface isentropic Mach number and free-stream Mach number.

It has also been predicted that capacity increases when the size of a pressure-side or suction-side trailing-edge cutback is increased. In the case of a pressure-side cutback this is probably because increasing cutback size increases the effective throat area. This is well-known to affect capacity linearly. In the case of a suction-side cutback the capacity changes are likely to originate from the aerodynamics downstream of the throat. This is concluded because the capacity

changes become negligible at choking pressure ratios, where information originating downstream of the throat cannot propagate upstream.

Additional investigations have been made into the effects of unsteady vortex shedding and trailing edge slot blowing rate on capacity and loss respectively. It has been concluded that unsteady effects have very little bearing on NGV capacity and that there is a blowing rate for which kinetic energy loss is minimal.

Manufacturing, measurement or prediction effects included 1) the effect of turbulence model choice, and 2) differences between 2D and 3D capacity predictions. Choice between the SST $k-\omega$ and Spalart-Allmaras turbulence models has been found to have a negligible effect on capacity predictions. However it has been found to have a significant effect on the predicted boundary layer separation point at the NGV trailing edge. This is a reminder that most RANS CFD solvers are unable to accurately predict separation.

It has also been found that significant differences exist between 2D and 3D capacity predictions. Given sets of NGVs with manufacturing variations, only 2D modelling has been able to isolate a relationship between geometric throat area and capacity. This is because non-midspan variations outweigh this effect in 3D. Only 3D modelling can predict the choking point of NGVs. This is because of span-wise variations in pressure ratio that delay choking. Overall, a combination of 2D and 3D analyses is essential for predicting how capacity is changed by manufacturing variations.

Bibliography

- [1] **I. Qureshi and T. Povey;** *Trent 900 EP1 HP NGV Capacity Measurement in Oxford Capacity Facility*; Rolls-Royce plc Technical Report DNS 177083; 2012
- [2] **T. Povey, M. Sharpe and A. Rawlinson;** *Experimental Measurements of Gas Turbine Flow Capacity Using a Novel Transient Technique*; ASME Journal of Turbomachinery 133; 2011
- [3] **I. V. Afanasiev, A. V. Granovski, A. M. Karelina and M. K. Kostege;** *The Problems of Flow Inaccuracy in Flow Capacity Definition by Using Different Numerical Techniques*; Journal of Thermal Science 13, no. 1; 2003
- [4] **I. V. Afanasiev, A. V. Granovski, A. M. Karelina and M. K. Kostege;** *Effect of 3D Vane Shape on the Flow Capacity*; ASME Paper GT2004-53095; 2004
- [5] **L. Fielding;** *The Effect of Irreversibility on the Capacity of a Turbine Blade Row*; 127-137, s.l. : Proceedings of the Institution of Mechanical Engineers 195; 1981
- [6] **D. K. Walters, J. H. Leyland;** *Impact of Film-Cooling Jets on Turbine Aerodynamic Losses*; ASME Journal of Turbomachinery 122. 537-545; 2000
- [7] **J. D. Denton, L. Xu;** *The Trailing Edge Loss of Transonic Turbine Blades*; ASME Journal of Turbomachinery 122, 277-285; 1990
- [8] **M. Deckers, J. D. Denton;** *The Aerodynamics of Trailing-Edge-Cooled Transonic Turbine Blades: Part 1 - Experimental approach*; ASME Paper 97-GT-518, 1997
- [9] **F. H. Kost, A. T. Holmes;** *Aerodynamic Effect of Coolant Ejection in the Rear Part of Transonic Rotor Blades*; AGARD CP-390, 41; 1985
- [10] **M. Raffel, F. Kost;** *Investigation of Aerodynamic Effects of Coolant Ejection at the Trailing Edge of a Turbine Blade by PIV and Pressure Measurements*; Experiments in Fluids 24, 447-461; Springer-Verlag; 1998

- [11] **J. H. Horlock**; *Axial Flow Turbines*; Robert E. Krieger Publishing Company, Malabar, USA; 1966
- [12] **S. M. Salim and S. C. Cheah**; *Wall $y+$ Strategy for Dealing with Wall-Bounded Turbulent Flows*; Proceedings of the IMECS 2009 vol. 2; 2009
- [13] **F. R. Menter**; *Zonal Two Equation $k-\epsilon$ Turbulence Models for Aerodynamic Flows*; AIAA Paper 93-2906; 1993
- [14] **P. R. Spalart and S. R. Allmaras**; *A One-Equation Turbulence Model for Aerodynamic Flows*; AIAA Paper 92-0439; 1992
- [15] **C. Hambridge**; *HP NGV Capacity*; PRS Transfer Report; Department of Engineering Science; University of Oxford; 2010
- [16] **G. Zamboni**; *Hydra CFD of the Trent 900 EP1 Turbine High Pressure Nozzle Guide Vane: Analysis of the Trailing Edge Slot Geometry Influence on Capacity Predictions Using GOM Scanned Data*; Rolls-Royce plc Technical Report DNS 181981; 2012
- [17] **T. Hall**; *Trent 900 Investigation of HP NGV Sensitivity to Trailing Edge Geometry*; Rolls-Royce plc Technical Report DNS 170140; 2011
- [18] **T. Povey**; *Effect of Film Cooling on Turbine Capacity*; ASME Journal of Turbomachinery 132-011901-1; 2009
- [19] **I. V. Afanasiev, A. V. Granovski, A. M. Karelina and M. K. Kostege**; *Effect of 3D Vane Shape on the Flow Capacity*; ASME Paper GT2004-53095; 2004
- [20] **F. Menter and Y. Egorov**; *The Scale-Adaptive Simulation Method for Unsteady Turbulent Predictions. Part 1: Theory and Model Description*; ANSYS Germany GmbH; 2010
- [21] **G. M. Laskowski and F. N. Felten**; *Steady and Unsteady CFD Simulations of Transonic Turbine Vane Wakes with Trailing Edge Cooling*; European Conference on Computational Fluid Dynamics; 2010
- [22] **V. Strouhal**; *On an Unusual Sort of Sound Excitation*; Annalen der Physik und Chemie, 3, 5(10), 216-251; 1878